
Article:
Zhang, L, Algeo, TJ, Zhao, L et al. (2024) Environmental and trilobite diversity changes during the middle-late Cambrian SPICE event. GSA Bulletin, 136 (1-2). pp. 810-828. ISSN: 0016-7606

https://doi.org/10.1130/B36421.1

Environmental and trilobite diversity changes during the middle-late Cambrian SPICE event

Lei Zhang[a*], Thomas J. Algeo[a, b, c], Laishi Zhao[a*], Tais W. Dahl[a, d], Zhong-Qiang Chen[a, b], Zihu Zhang[e,f], Simon W. Poulton[a, g], Nigel C. Hughes[h], Xueqing Gou[a], Chao Li[e,f]

[a] State Key Laboratory of Geological Processes and Mineral Resources, China University of Geosciences, Wuhan 430074, China

[b] State Key Laboratory of Biogeology and Environmental Geology, China University of Geosciences, Wuhan 430074, China

[c] Department of Geosciences, University of Cincinnati, Cincinnati, OH 45221-0013, USA

[d] GLOBE Institute, University of Copenhagen, DK-1350 Copenhagen, Denmark

[e] State Key Laboratory of Oil and Gas Reservoir Geology and Exploitation & Institute of Sedimentary Geology, Chengdu University of Technology, Chengdu 610059, China

[f] International Center for Sedimentary Geochemistry and Biogeochemistry Research, Chengdu University of Technology, Chengdu 610059, China

[g] School of Earth and Environment, University of Leeds, Leeds LS2 9JT, UK

[h] Department of Earth and Planetary Sciences, University of California, Riverside, CA 92521, USA

* Corresponding author: Lei Zhang, email: zhanglei_cug@sina.com

Abstract

The Steptoean Positive Carbon Isotope Excursion (SPICE) event at ~497-494 Ma was a major carbon-cycle perturbation of the late Cambrian that coincided with rapid diversity changes among trilobites. Several scenarios (e.g., climatic/oceanic cooling, and seawater anoxia) have been proposed to account for an extinction of trilobites at the onset of SPICE, but the exact mechanism remains unclear. Here, we present a chemostratigraphic study of carbonate carbon and carbonate-associated sulfate sulfur isotopes ($\delta^{13}C_{carb}$ and $\delta^{34}S_{CAS}$) and elemental redox proxies (U_{EF}, Mo_{EF}, and C_{org}/P), augmented by secular trilobite diversity data, from both upper slope (Wangcun) and lower slope (Duibian) successions from the Jiangnan Slope, South China, spanning the Drumian to lower Jiangshanian. Redox data indicate locally/regionally well-oxygenated conditions throughout the SPICE event in both study sections except for low-oxygen (hypoxic) conditions within the rising limb of the SPICE (early-middle Paibian) at Duibian. As in coeval sections globally, the reported $\delta^{13}C_{carb}$ and $\delta^{34}S_{CAS}$ profiles exhibit first-order coupling throughout the SPICE event, reflecting co-burial of organic matter and pyrite controlled by globally integrated marine productivity, organic preservation rates and shelf hypoxia.

Increasing $\delta^{34}S_{CAS}$ in the 'Early SPICE' interval (late Guzhangian) suggests that significant environmental change (e.g., global-oceanic hypoxia) was underway before the global carbon cycle was markedly affected. Assessment of trilobite range data within a high-resolution biostratigraphic framework for the middle-late Cambrian facilitated re-evaluation of the relationship of the SPICE to contemporaneous biodiversity changes. Trilobite diversity in South China declined during the Early SPICE (corresponding to the End-Marjuman Biomere Extinction, or EMBE, of Laurentia) and at the termination of the SPICE (corresponding to the End-Steptoean Biomere Extinction, or ESBE, of Laurentia), consistent with biotic patterns from other cratons. We infer that oxygen minimum zone (OMZ) and/or shelf hypoxia expanded as a result of locally enhanced productivity due to intensified upwelling following climatic cooling, and that expanded hypoxia played a major role in the EMBE at the onset of SPICE. During the SPICE event, global-ocean ventilation promoted marine biotic recovery, but termination of SPICE-related cooling in the late Paibian may have reduced global-ocean circulation, triggering further redox changes that precipitated the ESBE. Major changes in both marine environmental conditions and trilobite diversity during the late Guzhangian demonstrate that the SPICE event began earlier than the Guzhangian-Paibian boundary, as previously proposed.

Keywords: carbon isotopes; sulfur isotopes; oceanic anoxia; species diversity; Marjuman Biomere; Steptoean Biomere

1. Introduction

The Cambrian, a key period in Earth history, was characterized by the Cambrian Explosion of marine invertebrate life (Marshall, 2006) as well as unstable marine environments as revealed by fluctuations in carbon isotopes (Saltzman and Thomas, 2012), multiple biotic extinctions, and the development of extreme environmental conditions (Servais et al., 2010). The Steptoean Positive Carbon Isotope Excursion (SPICE) was the last major carbon isotope excursion (CIE) of the Cambrian (Saltzman et al., 1998, 2000), recording a shift of ~4 to 6‰ in marine carbonate carbon isotopes ($\delta^{13}C_{carb}$) for an interval of 3.0 ± 0.2 Myr during the Paibian Stage (~497–494 Ma; lowermost Furongian Series; Sørensen et al., 2020; see Supplemental Section 1 for Cambrian timescale). The SPICE event began at the base of the Paibian Stage, as defined by the first appearance datum (FAD) of the trilobite *Glyptagnostus reticulatus* (Peng and Robison, 2000; Zhu et al., 2018), and continued to the base of the *Irvingella major* Zone in the early Jiangshanian (Peng et al., 2004, 2012; Gerhardt and Gill, 2016), thus spanning from the middle Cambrian (Miaolingian, formerly Series 3) to the late Cambrian (Furongian) series boundary interval.

The SPICE event was associated with a pronounced marine biotic turnover, including extinctions of trilobites and agnostid arthropods (Palmer, 1984; Saltzman et al., 2000; Gerhardt and Gill, 2016; Moysiuk and Caron, 2019; Zhang et al., 2021) and brachiopods (Rowell and Brady 1976; Rieboldt, 2005), changes in the composition of reef communities (Lee et al., 2015), and large increases in plankton diversity (Servais et al., 2008). Middle and upper Cambrian trilobites

have been especially well studied, and the SPICE event was accompanied by extinctions of the Marjumiid Biomere at the end of the Guzhangian Stage and the Pterocephaliid Biomere in the early Jiangshanian Stage (Palmer, 1979, 1984; Gerhardt and Gill, 2016; Zhang et al., 2021). Several mechanisms have been proposed to explain the extinction of the Marjumiid Biomere, including global temperature changes (Lochman-Balk, 1970; Öpik, 1966), a rise in the thermocline and shelf cooling (Stitt, 1975), and/or ecospace changes linked to sea-level fluctuations (Ludvigsen, 1982; Westrop, 1988; Westrop and Ludvigsen, 1987). Geochemical studies have confirmed some of these inferences and proposed other potential causes, for example, upwelling of cool deep waters onto shallow shelves (Perfetta et al., 1999; Elrick et al., 2011) as well as widespread oceanic anoxia (Saltzman et al., 1998; Hurtgen et al., 2009; Gill et al., 2011; 2021; Dahl et al., 2014). However, these studies are based on geographically limited datasets containing a small number of proxies, rendering the causes of the extinction uncertain.

Middle-Late Cambrian trilobite extinctions were almost certainly linked to marine environmental changes, but the nature of such changes during the SPICE event remains poorly known. The SPICE is thought to have coincided with a major phase of global cooling, although this inference is based largely on carbon-cycle changes and physical evidence of sea-level fall rather than direct temperature measurements. In addition to a positive CIE, changes in the global carbon cycle are indicated by evidence of enhanced marine productivity and organic carbon burial from organic carbon-nitrogen isotopes (Hammer and Svensen, 2017), carbon-sulfur isotope modeling of atmospheric O_2 content (Saltzman et al., 2011; Krause et al., 2018), N/P ratios indicating P limitation of marine productivity (Saltzman, 2005), and a decrease in seawater $^{87}Sr/^{86}Sr$ values (Zhang et al., 2020). Physical evidence of cooling includes a sea-level lowstand at the Sauk-II/III contact (= mid-Paibian) (Saltzman et al., 2000, 2004; Sørensen et al. 2020), ice-erosional features at mid-latitudes of Baltica (Dronov and Popov 2004; Cherns and Wheeley, 2009), consistent with growth of continental icesheets during the early to middle Paibian (Matthews and Al-Husseini, 2010; Al-Husseini, 2017). Due to the indirect nature of this evidence, climate cooling during the early to middle Paibian remains contentious. The only oxygen isotope ($\delta^{18}O$) study of the Paibian to date documented increased sea-surface temperatures on the western margin and cratonic interior of Laurentia (Elrick et al., 2011; Wotte et al., 2019). However, this warming event is likely to have been a local signal related to shallowing on a tropical continental shelf, with glacio-eustatic fall causing the study sections to shallow into the ocean-surface layer, thus recording locally warmer conditions despite the general climatic cooling necessary to induce glacial expansion.

In the present study, our goals are to examine chemostratigraphic records of marine paleoenvironmental change during the SPICE, and to link these changes to contemporaneous records of trilobite diversity in order to better understand controls on Middle-Late Cambrian biotic events. We analyzed two middle to upper Cambrian sections in South China, Wangcun and Duibian, representing relatively shallower (upper slope) and deeper (lower slope) depositional settings, applying elemental redox proxies (i.e., U_{EF}, Mo_{EF}, C_{org}/P) to track local environmental

changes that may have affected biodiversity patterns, and inorganic carbon and sulfur isotopes (i.e., $\delta^{13}C_{carb}$ and $\delta^{34}S_{CAS}$; carb = carbonate; CAS = carbonate-associated sulfate) as global seawater proxies. Furthermore, we reprocessed published trilobite data for these two sections, which are among the faunally best studied successions of middle to late Cambrian age globally, having yielded a wealth of trilobite taxonomic data suitable for analysis of biodiversity trends. Our study thus provides an integrated geochemical and paleontological dataset that addresses fundamental relationships between paleoenvironmental changes and biotic evolution during the SPICE event.

2. Geological background

2.1. Paleogeography

During the middle and late Cambrian, the South China Craton was located on the equatorial margin of Gondwana (Fig. 1A). Three main depositional environments existed along a platform-to-basin transect, with a shallow-platform carbonate facies to the northwest (Yangtze Platform), argillaceous carbonate and shale in the central slope facies (Jiangnan Slope), and fine-grained siliciclastic and chert in the basinal facies (Nanhua Basin) to the southeast (Fig. 1B; Feng et al., 2002; note: all coordinates are modern unless otherwise noted). The present study sections are located on the Jiangnan Slope (Zuo, et al., 2018).

2.2. Wangcun section

Wangcun (GPS: 28°43′2.84″ N, 109°58′26.10″ E) is an outcrop section exposed along a roadcut on the northern bank of the Youshui River in western Hunan Province, South China (Fig. 1C). It is a parastratotype of the Drumian-Guzhangian stage boundary, for which the Global Stratotype Section and Point (GSSP) is the Luoyixi section, which is located on the southern bank of the same river (Peng et al., 2004, 2005, 2009). The Wangcun section consists, in ascending order, of the Aoxi, Huaqiao, and Shenjiawan formations. The Aoxi Formation is mainly composed of dolomite and black shale interbedded with limestone; the Huaqiao Formation is dominated by thin-bedded muddy limestone, with a few oolitic limestone beds in the lower part, and thick-bedded mudstone containing lenticular limestone, conglomeratic limestone, and calcareous shale beds in the upper part; and the Shenjiawan Formation consists of limestone and dolomitic limestone (Peng et. al., 2004; Fig. 2).

The trilobite biostratigraphy of the Wangcun section is well studied for the Drumian and Guzhangian stages, but less so for the Paibian and Jiangshanian stages (Fig. 2A). A total of 9 trilobite zones have been established, in ascending order, the *Ptychagnostus atavus*, *Pt. punctuosus*, *Goniagnostus nathorsti*, *Lejopyge armata*, *L. laevigata*, *Proagnostus bulbus*, *Linguagnostus reconditum*, *Glyptagnostus stolidotus*, and *G. reticulatus* zones. The bases of the Drumian, Guzhangian, and Paibian stages are defined by the first appearance datums (FADs) of the trilobites *P. atavus*, *L. laevigata*, and *G. reticulatus*, respectively (Peng, 2005; Peng et al., 2009). The placement of the top of the *G. reticulatus* Zone and the stratigraphic interval of the *Ag. orientalis* Zone (note: the base of this zone is equivalent to the base of the Jiangshanian) are

155 defined based on correlations with Duibian A (Zuo et al., 2018).
156
157 *2.3. Duibian section*
158 The Duibian section consists of outcrops near Duibian village, 10 km north of Jiangshan City,
159 western Zhejiang Province, South China (Fig. 1D). Dubian A (GPS: 28°48′48.38″ N, 118°37′19.21″
160 E), a parastratotype of the Paibian-Jiangshanian stage boundary, contains, in ascending order, the
161 upper Yangliugang, Huayansi, and lower Siyanshan formations (Lu and Lin, 1989; Peng et al.,
162 2012). The Yangliugang Formation consists mainly of dark-gray, thin-bedded dolomitic limestone
163 with calcareous mudstone interbeds; the Huayansi Formation comprises dark, thin-bedded
164 limestone with thin shale interbeds and light-colored ribbon limestones; and the Siyangshan
165 Formation consists of pale limestone with breccias in the lower part, and light gray thin-bedded
166 limestone interbedded with calcareous mudstone and muddy limestone in the upper part. Duibian
167 B (28°48′46.14″ N, 118°37′17.20″ E), the GSSP for the Paibian-Jiangshanian stage boundary, is
168 located ~250 m to the south of Duibian A and exposes only a part of the Huayansi Formation (Fig.
169 1D). Although their chemostratigraphic profiles are shown separately in the figures of this study,
170 the geochemical datasets of Duibian A and B were combined for purposes of statistical evaluation
171 owing to their proximity and general similarity.
172 The trilobite biostratigraphy of the Duibian section (Figs. 3A, 4A) is well established (Lu and
173 Lin, 1989; Peng et al., 2012). At Duibian A, the bases of the Paibian and Jiangshanian stages are
174 defined by the FADs of the trilobites *Glyptagnostus reticulatus* and *Agnostotes orientalis*,
175 respectively. Duibian B is the GSSP of the base of the Jiangshanian Stage, based on the FAD of
176 the trilobite *Ag. orientalis* (Peng et al., 2012). The base of the Jiangshanian Stage was placed at
177 116.6 m and 108.12 m above the base of the Huayansi Formation at Duibian A and B, respectively
178 (Peng et al., 2012).
179
180 *2.4. Comparative global sections*
181 Results from the study sections were compared with geochemical data from five widely
182 distributed SPICE sections (Fig. 1A). Four of these auxiliary sections accumulated on continental
183 shelves, ranging from subtidal-peritidal to deep-shelf settings: (1) Lawson Cove, Utah (Gill et al.,
184 2011; note: not "Lawsons Cove" as given in that source); (2) Shingle Pass, Nevada (Saltzman et
185 al., 1998; Gill et al., 2007); (3) Mount Whelan core, Australia (Saltzman et al., 2000; Gill et al.,
186 2011); and (4) TE-1 core, Texas County, Missouri (Gill et al., 2011). The fifth auxiliary section,
187 the Andrarum-3 core (Sweden), was deposited below storm wave base (Gill et al., 2011; Dahl et
188 al., 2013). Paired $\delta^{13}C_{carb}$ and $\delta^{34}S_{CAS}$ values for the five auxiliary sections, as well as local/global
189 redox proxy data for two of the five sections (i.e., carbonate uranium isotopes from Mount Whelan
190 core, and redox sensitive elements from Andrarum-3 core) were available for comparisons (note:
191 the other three auxiliary sections lack such data). See Supplemental Section 2 and Table S1 for
192 more paleogeographic and stratigraphic background information about the study and auxiliary
193 sections, and Supplemental Figure S1 for correlation of trilobite zones between South China and

194 Laurentia.
195
196 *2.5. Internal stratigraphy of the SPICE event interval*
197 Previous studies have divided the SPICE interval into two parts: a 'rising limb' marked by an
198 increasing trend of carbonate carbon isotopes ($\delta^{13}C_{carb}$), and a 'falling limb' marked by a
199 decreasing $\delta^{13}C_{carb}$ trend (Saltzman et al., 2000; Pulsipher et al., 2021). In the present study, we
200 identify a third interval that we term 'Early SPICE', marking the earliest stage of the SPICE event
201 prior to a major rise in $\delta^{13}C_{carb}$. In addition, for the sake of ease of reference, we term the intervals
202 that preceded and followed the SPICE event the 'Pre-SPICE' and 'Post-SPICE', respectively. In
203 our study sections, the Pre-SPICE, Early SPICE, Rising SPICE (= 'rising limb'), Falling SPICE (=
204 'falling limb'), and Post-SPICE intervals correspond to Units I to V (in sequence). For sections
205 having a substantial Pre-SPICE interval, we have designated the somewhat older carbon isotope
206 excursion known as DICE (Drumian Carbon Isotope Excursion) as Unit Ia and the strata between
207 DICE and the base of the Early SPICE as Unit Ib. All five units are present at Wangcun (Fig. 2C),
208 but only four units (Ib, II, III and IV) are present at Duibian A (Fig. 3C), and only two units (IV
209 and V) at Duibian B (Fig. 4C).
210 The five intervals described above were defined primarily on the basis of carbonate carbon
211 isotope ($\delta^{13}C_{carb}$) variation (cf. Saltzman et al., 2000; Pulsipher et al., 2021) but with reference to
212 some secondary criteria including the $\delta^{34}S_{CAS}$ profile and trilobite range data. To facilitate use in
213 other studies, we define the subdivisions primarily in terms of carbon isotope variation and
214 trilobite range data. The Early SPICE interval is marked by a gentle rise of $\delta^{13}C$ (note: not the
215 steep rise associated with the Rising SPICE), or, in sections lacking such a $\delta^{13}C$ feature, by a
216 significant rise of $\delta^{34}S_{CAS}$, during the late to latest Guzhangian Stage (*Linguagnostus reconditus*
217 and *G. stolidotus* zones). The transition from the Early SPICE to Rising SPICE is marked by a
218 sharp acceleration in the $\delta^{13}C$ profile, or by the onset of rising $\delta^{13}C$ in sections lacking the slow
219 $\delta^{13}C$ rise of the Early SPICE; it spans the earliest Paibian (base of *G. reticulatus* Zone) to middle
220 Paibian Stage (*A. inexpectans* Zone). The transition from the Rising SPICE to Falling SPICE is
221 marked by the shift from increasing to decreasing $\delta^{13}C$ values; in some sections (e.g., Shingle Pass,
222 Lawson Cove, TE-1 Texas County Core, Mount Whelan Core; Saltzman et al., 1998, 2000; Gill et
223 al., 2007, 2011) this transition is rapid, but in other sections (e.g., Deogwoo, Wa'ergang, House
224 Range; Baker, 2010; Chung et al., 2011; Li et al., 2018) there is an extended plateau of nearly
225 uniform high $\delta^{13}C$ values that makes identification of the exact point of the transition somewhat
226 arbitrary. The Falling SPICE corresponds to the middle Paibian to early Jiangshanian Stage (i.e., *A.*
227 *inexpectans* Zone to lower part of *Ag. orientalis* Zone). The Pre-SPICE and Post-SPICE are
228 defined simply as those intervals preceding onset of the Early SPICE and following termination of
229 the Falling SPICE, respectively. The Post-SPICE corresponds to middle-late Jiangshanian Stage
230 (i.e., upper part of *Ag. orientalis* Zone to *Eolotagnostus* Zone).
231 Our scheme for internal subdivision of the SPICE event redefines the timing of its onset.
232 Earlier studies placed the base of the SPICE event at the onset of the sharp rise in the $\delta^{13}C_{carb}$

profile (e.g., Saltzman et al., 2000; Zhu et al., 2018; Pulsipher et al., 2021; but note that Schiffbauer et al., 2017 proposed a globally diachronous onset of the SPICE), which is equivalent to the base of the Rising SPICE of our study. However, the present study demonstrates that the former definition is inconvenient for three reasons. First, the Wangcun and Duibian sections show positive shifts in $\delta^{13}C_{carb}$ and $\delta^{34}S_{CAS}$ heralding the SPICE event well below the Guzhangian-Paibian boundary, which has previously defined the base of the SPICE (Saltzman et al., 2000). At Wangcun, obvious positive shifts commence at ~210 m, or ~70 m below the base of the Rising SPICE (which is at ~280 m), and at Duibian A, obvious positive shifts commence at ~−4 m, or ~11 m below the base of the Rising SPICE (which is at ~7 m; Figs. 2-3). Second, the concurrent positive shifts of $\delta^{13}C_{carb}$ and $\delta^{34}S_{CAS}$ during the late Guzhangian Stage were a global phenomenon (Gill et al., 2007; Pulsipher et al., 2021), and they coincided with the initiation of shifts in other global proxies (e.g., $\delta^{238}U$ values) that continued into the Rising SPICE interval (Dahl et al., 2014). Third, the former definition decouples the SPICE from the EMBE, leading to suggestions that the EMBE had non-SPICE-related causes (Palmer, 1984; Saltzman et al., 2000; Elrick et al., 2011), which we regard as almost certainly incorrect. For these reasons, we propose redefinition of the base of the SPICE based on the onset of paleo-environmental disturbances as determined from multiple proxies (i.e., $\delta^{13}C_{carb}$, $\delta^{34}S_{CAS}$, $\delta^{98}Mo$ and $\delta^{238}U$), instead of a single proxy ($\delta^{13}C_{carb}$) that exhibits invariant or regionally variable values during the EMBE (e.g., Gerhardt and Gill, 2016; Schiffbauer et al., 2017). The interval of slowly rising $\delta^{13}C_{carb}$ during the earliest part of the redefined SPICE is herein termed the "Early SPICE" interval (Unit II of present study, within the *Li. reconditus* and *G. stolidotus* zones) (Figs. 2-3). This redefinition places the onset of the SPICE event in the late Guzhangian rather than at the Guzhangian-Paibian stage boundary (cf. Saltzman et al., 2000), and it links middle-late Cambrian trilobite diversity changes more effectively to the trajectory of the SPICE event (cf. Gerhardt and Gill, 2016; Zhang et al., 2021).

3. Methods

3.1. Isotopic and elemental analyses

Weathered surfaces and diagenetic veins were trimmed off, and the remaining bulk-rock carbonate was powdered to <74 μm (200 mesh) using a rock mill. Major elements were measured using wavelength-dispersive XRF and trace elements using ICP-MS, after sample powder digestion by HNO_3 and HF, in the State Key Laboratory of Geological Processes and Mineral Resources at the China University of Geosciences–Wuhan. Average analytical uncertainty is better than 5% (RSD) for major elements based on repeated analysis of national standards GBW07132, GBW07133 and GBW07407, and better than 2% (RSD) for trace elements based on international standards AGV-2, BHVO-2, BCR-2 and GSR-1. In the same laboratory, total organic carbon (TOC) content was measured using an Elementar Vario Micro Cube Analyzer, and inorganic carbon isotopes were measured using a 253 Plus Isotope Ratio Mass Spectrometer (IR-MS) interfaced with a Kiel IV auto-sampler. The analytical precision was better than 0.04‰

for both $\delta^{13}C_{carb}$ and $\delta^{18}O_{carb}$ based on duplicate analyses of national standards GBW-04416 and GBW-04417. Multiple NaCl rinses (generally > 30 times) was applied to extract carbonate-associated sulfate (CAS) (Wotte et al., 2012). Sulfur isotopes in CAS were analyzed using a Delta V plus IR-MS in the State Key Laboratory of Biogeology and Environmental Geology at the China University of Geosciences–Wuhan. Analytical errors were 0.08 ‰, 0.09 ‰ and 0.20 ‰ (1σ), respectively, calculated from duplicate analyses of the international standards NBS 127, IAEA SO-5, and IAEA SO-6. Detailed descriptions of all methods are given in Supplemental Section 3.

3.2. Trilobite biodiversity

Trilobite biostratigraphic analyses at Wangcun were carried out by Peng and Robison (2000) and Peng et al. (2009), during investigation of the nearby Luoyixi section as the GSSP of the base of the Guzhangian Stage. A total of 66 species (including 2 undefined species) were recognized from ~90 stratal levels at Wangcun, including within the Pre-SPICE and Early SPICE intervals (~150- and ~100-m-thick, respectively), and the lower part of the Rising SPICE (20-m-thick).

Trilobite biostratigraphic work at Duibian was carried out by Lu and Lin (1989) and Peng et al. (2006, 2009, 2012) before designation of this locale as the GSSP of the base of the Jiangshanian Stage. A total of 64 species (including 14 undefined species) were recognized from ~50 stratal levels within a ~200-m-thick interval containing the SPICE event at Duibian A, and 35 species (including 9 undefined species) from ~30 stratal levels within a ~40-m-thick interval at Duibian B.

In the present study, we compiled trilobite species range data in order to construct both species diversity and range-through diversity profiles for each study section for the lowermost Drumian to lower Jiangshanian interval. The *species diversity curve* shows the total number of trilobite species actually identified at a given stratal level in the source studies (Peng and Robison, 2000; Peng et al., 2004, 2005, 2006, 2009, 2012). The *range-through diversity curve* accounts for taxa that are absent at a given stratigraphic level but present in both underlying and overlying horizons, on the assumption that their absence in such cases is due to incompleteness of the fossil record.

4. Results

4.1. *Variations of isotopic and elemental proxies*

The $\delta^{13}C_{carb}$ profiles of the study sections exhibit a broad first-order positive excursion representing the SPICE, spanning a stratigraphic interval of 229.0 m to 361.0 m at Wangcun and −4.0 m to 29.0 m at Duibian A-B (Figs. 2-4). From background values of ~0-1 ‰ (Unit Ib; Pre-SPICE), the excursion began in the late Guzhangian with a slow initial shift that was slightly larger at Wangcun (~+1 ‰) relative to Duibian A (~+0.5 ‰) (Unit II; Early SPICE). A steeper rise in $\delta^{13}C_{carb}$ commenced at the Guzhangian-Paibian boundary, marking the onset of the main phase of SPICE (Unit III; Rising SPICE). The positive excursion peaked in the middle Paibian with

values of +3.84 ‰ at Wangcun and +3.15 ‰ at Duibian A. $\delta^{13}C_{carb}$ values declined during the late Paibian to early Jiangshanian (Unit IV; Falling SPICE), stabilizing at ~1 ‰ in the Post-SPICE interval (Unit V). The full SPICE excursion appears relatively smoother at Wangcun than at Duibian, where some small-scale variability is present (e.g., in Unit III), although this difference may be due to the higher-resolution sampling of the latter section.

The $\delta^{34}S_{CAS}$ profiles of the study sections also show first-order positive excursions during the SPICE (Figs. 2-4). Following background values of ~25-35 ‰ in the Pre-SPICE, a major rise of $\delta^{34}S_{CAS}$ begins in the Early SPICE, reaching a peak value that is slightly higher at Wangcun (+48.4 ‰) relative to Duibian A (+46.9 ‰). Relatively stable plateau values are observed at Wangcun (~+40-50 ‰) and Duibian A (~+35-45 ‰) in the Rising SPICE, but $\delta^{34}S_{CAS}$ shows a decreasing trend to a minimum of ~+28 ‰ (Wangcun) and ~+20-25 ‰ (Duibian) by the end of the Falling SPICE. $\delta^{34}S_{CAS}$ fluctuates within ~5-25 ‰ and finally maintains stable values (~25-30 ‰) in the Post-SPICE at Wangcun, with a comparable range of fluctuations (within ~15-35 ‰) at Duibian B.

The TOC profile at Wangcun shows a roughly decreasing trend from ~0.6 to ~0.2 wt.% with a few peak values (to ~0.6-1.0 wt.%) in the DICE to Early SPICE intervals, then maintains relatively low values (~0.2 wt.%) punctuated by several sharp peaks (to ~0.6-1.4 wt.%) in the Rising to Post-SPICE intervals (Fig. 5B). The TOC profiles show more regular variations at Duibian, stabilizing around 0.10 wt.% in the Pre-SPICE, rising to relatively higher level (~0.2 wt.%) with few peak values (~0.5-2.0 wt.%) in the Rising SPICE, then gradually dropping in the Falling SPICE and reaching a minimum of ~0.02 wt.% by its termination, before sharply rising to a peak value ~0.4 wt.% and fluctuating over ~0.1-0.8 wt.% in the Post-SPICE (Fig. 6B, 7B).

The C_{org}/P profile at Wangcun exhibits low values (mostly < 5) in the DICE and Early SPICE, then rises to relatively higher values of ~60-80 in the Early and Rising SPICE, followed by a return to lower values of ~0-50 in the Falling SPICE, before fluctuating in the range of ~0-100 in the Post-SPICE (Fig. 5F). At Duibian, relative to background values (~0-20) in the Pre-SPICE, C_{org}/P rises progressively to ~30 in the Early SPICE, then remains at a plateau (~25-45) punctuated by several peaks (to ~50-200) in the Rising SPICE, before gradually dropping to minimum values (< 5) in the Falling SPICE, and finally rebounding to relatively higher values (~15-45) in the Post-SPICE (Fig. 6F, 7F).

Trace-element enrichment factors (EFs) were calculated as $X_{EF} = (X/Al)_{sample} / (X/Al)_{UCC}$, where UCC is average upper crustal composition (McLennan, 2001). In order to reduce variance in EFs related to small denominator values, only samples with Al > 0.5% were used in redox reconstructions (Figs. 5-7; see also Supplemental Fig. S3). At Wangcun, the U_{EF} and Mo_{EF} profiles exhibit decreasing trends from ~15 to ~3 and ~64 to ~1, respectively, in the DICE to Pre-SPICE intervals, and then both profiles exhibit lower values (mostly < 3) in the Early SPICE to Post-SPICE (Fig. 5D-E). At Duibian A, the U_{EF} profile shows a decreasing trend (~7 to ~2) in the Pre-SPICE to Early SPICE, followed by stable values (~3-5) in the Rising SPICE, before increasing (to >10) in the Falling SPICE (Fig. 6D). The Mo_{EF} profile mostly exhibits low values

(~< 3) in the Pre-SPICE to Early SPICE, then rises to slightly higher values (~3 to ~9) in the Rising SPICE, before dropping to a minimum (~1) in the Falling SPICE (Fig. 6E). At Duibian B, U_{EF} fluctuates between ~2 and ~17, and Mo_{EF} between ~1 and ~10, in the Falling SPICE to Post-SPICE interval (Fig. 7D-E).

4.2. Trilobite species diversity records

At Wangcun, trilobite range-through species diversity rises from 2 to 9 at ~30-80 m (i.e., within the *Ptychagnostus aculeatus* Zone), remains stable (~5) at ~80-150 m (i.e., lower part of the Pre-SPICE), followed by a slight increase to ~10-15 at ~220 m (i.e., upper part of the Pre-SPICE), before a significant decrease to a minimum of 1 at ~270 m (base of the *G. stolidotus* Zone, i.e., the EMBE), and with the minimum value continuous into the Rising SPICE (base of the *G. reticulatus* Zone) (Fig. 2).

At Duibian A, trilobite range-through species diversity rises significantly from < 10 at the base of the section (lower Guzhangian) to a maximum value of 25 at –5 m prior to the onset of the Early SPICE (base of the *Li. reconditus* Zone) (Fig. 3). Between –5 m and 0 m (base of the *G. stolidotus* Zone, i.e., EMBE), range-through species diversity drops sharply to < 5, followed by a gradual decline to 0 at 30 m, representing the end of the Rising SPICE (lower part of the *A. inexpectans* Zone). Upwards, range-through species diversity gradually rises to ~5-10 at 70 m (end of Falling SPICE) before a decline to < 5 at the top of the section (within the *Ag. orientalis* Zone, i.e., ESBE). At Duibian B, trilobite range-through species diversity gradually increases from 0-5 at the base of the section to a maximum of 15 at 28 m (end of the Falling SPICE; upper part of the *A. inexpectans* Zone), followed by a decrease to < 5 at 35-40 m (i.e., ESBE) within the Post-SPICE interval at the top of the section (middle part of the *Eolotagnostus* Zone) (Fig. 4).

5. Discussion

5.1. Data evaluation

5.1.1. CAS extraction methods

The extraction method of CAS (i.e., using multiple NaCl rinses) that we applied in the present study is likely to remove a large part of the contaminant secondary sulfate, for example, that from soluble and organically bound sulfur as well as diagenetically oxidized pyrite. Repeated leaching with an NaCl solution is recommended as a standard step in CAS extraction from carbonate rocks, as it can fully remove non-CAS sulfate that was not incorporated into the carbonate mineral structure. It is superior to using NaOCl or H_2O_2 rinses alone, or a combination thereof with NaCl rinses (Wotte et al., 2012). We generally repeated NaCl rinses at least 30 times, which is more effective than a small number of NaCl rinses or a single NaCl rinse followed by an NaOCl rinse (Edwards et al., 2019), as the latter two methods are unlikely to fully remove non-CAS sulfate. Although [CAS] is low in Duibian samples (~1-4 ppm), making $\delta^{34}S_{CAS}$ susceptible to the influence of oxidized pyrite prior to or during laboratory pretreatment, we infer that such effects were probably minor because the $\delta^{34}S_{CAS}$ profiles of the study sections exhibit

relatively high values (mostly > 20 ‰) relative to those of pyrite sulfur (< ~−10 ‰) as well as stable stratigraphic trends without anomalous negative outliers.

5.1.2. Effects from local depositional conditions and early marine diagenesis

Local depositional conditions and early marine diagenesis determine preservation of marine carbonate and regional/global stratigraphic expressions of carbon-isotopic signals in shallow-water carbonate facies. Large glacio-eustatic fluctuations can result in isotopic shifts unrelated to variations in the global carbon cycle (Swart, 2008, 2015; Swart and Kennedy, 2012). For example, flooding of carbonate platforms can increase the proportion of aragonite in sediments, resulting in a globally synchronous positive $\delta^{13}C$ excursion. Conversely, sea-level fall results in exposure of platform carbonates to freshwater, leading to meteoric diagenetic alteration in which enhanced authigenic carbonate precipitation can generate a negative $\delta^{13}C$ excursion (Schrag et al., 2013; Zhao et al., 2016). However, the positive $\delta^{13}C_{carb}$ excursion of the SPICE event was associated with a major sea-level fall (e.g., Saltzman et al., 2000), arguing against the influence of sea-level variation on marine carbonate carbon-isotopic compositions. Previous studies have inferred that the SPICE was facies-dependent, through intrusion of ^{13}C-enriched deepwaters onto carbonate platforms during sea-level rise (Schiffbauer et al., 2017). However, the recognition of the Early SPICE interval in the present study suggests that the influence of facies on carbon-isotopic compositions was weak. In addition, regional anoxia-euxinia generally corresponds to positive $\delta^{13}C_{carb}$ excursions during the SPICE (e.g., Gill et al., 2011), indicating that the influence of authigenic carbonates was limited.

Local depositional conditions and early marine diagenesis determine the preservation of primary $\delta^{34}S_{CAS}$ signals (Present et al., 2019; Richardson et al., 2019, 2021). Generally, low and stable $\delta^{34}S_{CAS}$ values are associated with deep-water facies, whereas higher and more variable values characterize shallow-water facies (Richardson et al., 2019). For example, carbonate rocks deposited in slope facies may incorporate sulfate from anoxic marine-phreatic pore fluids that have been isotopically modified from seawater by microbial sulfate reduction (Present et al., 2019). In the present study, Wangcun and Duibian are located in slope areas in which oxic-suboxic conditions prevailed (see Section 5.2.1), suggesting that the influence of facies on $\delta^{34}S_{CAS}$ signals was limited. However, facies-related influences on $\delta^{34}S_{CAS}$ signals may have been pronounced in deep-water SPICE successions such as TE-1 Texas County Core (Gill et al., 2011), which is characterized by $\delta^{34}S_{CAS}$ that is ~10 to 20 ‰ lower than in shallow-water successions such as the Mount Whelan Core (see Supplementary Information). Moreover, $\delta^{34}S_{CAS}$ profiles exhibit variable values in slope sections globally (see Section 5.3), suggesting potential facies or geographic dependency of primary $\delta^{34}S_{CAS}$ signals during the SPICE event.

5.1.3. Diagenetic alteration

The present $\delta^{13}C_{carb}$ profiles are interpreted as primary marine signals based on relationships with $\delta^{18}O_{carb}$ and Mn/Sr ratios (see Supplemental Fig. S2). Generally, Mn/Sr ratios > ~2 and strong

covariation with Mn/Sr or $\delta^{18}O_{carb}$ are taken as evidence of diagenetic alteration in carbonate rocks (Marshall, 1992; Brand, 2004). At Wangcun and Duibian, Mn/Sr ratios are low (avg. 0.41 ± 0.33, 0.1 ± 0.07 and 0.06 ± 0.06, respectively), consistent with little to no diagenetic alteration of the samples. Moreover, $\delta^{13}C_{carb}$ shows only weak correlation to Mn/Sr ($r = -0.32$, $n = 37$, $p(\alpha) < 0.05$; $r = -0.39$, $n = 100$, $p(\alpha) < 0.01$, respectively), and none correlation to $\delta^{18}O_{carb}$ ($r = -0.13$, $n = 48$, $p(\alpha) > 0.10$; $r = -0.11$, $n = 130$, $p(\alpha) > 0.10$, respectively).

Primary marine $\delta^{34}S_{CAS}$ signals were further evaluated based on relationships to $\delta^{18}O_{carb}$, Mn/Sr, Mg/Ca, and CAS concentrations (see Supplemental Fig. S2). Generally, diagenetic alteration and dolomitization of carbonate rocks produces strong covariation between $\delta^{34}S_{CAS}$, $\delta^{18}O_{carb}$, Mn/Sr and Mg/Ca (cf. Marenco et al., 2008). However, such effects are not evident at Wangcun or Duibian, because $\delta^{34}S_{CAS}$ shows weak or no relationship to $\delta^{18}O_{carb}$ ($r = -0.17$, $n = 34$, $p(\alpha) > 0.10$; $r = -0.24$, $n = 81$, $p(\alpha) < 0.05$, respectively), Mn/Sr ($r = -0.45$, $n = 34$, $p(\alpha) < 0.01$; $r = -0.01$, $n = 81$, $p(\alpha) > 0.10$, respectively) and Mg/Ca ($r = 0.00$, $n = 34$, $p(\alpha) > 0.10$; $r = -0.34$, $n = 81$, $p(\alpha) < 0.01$, respectively). Although $\delta^{34}S_{CAS}$ may become coupled to CAS concentrations through diagenetic, dolomitization or chemical extraction processes (Marenco et al., 2008; Wotte et al., 2012), the lack of $\delta^{34}S_{CAS}$-CAS relationships at Wangcun and Duibian ($r = -0.28$, $n = 34$, $p(\alpha) > 0.10$; $r = -0.19$, $n = 81$, $p(\alpha)$ ~0.05, respectively) is consistent with little to no post-depositional alteration. Additionally, $\delta^{34}S_{CAS}$ variations during the SPICE are similar to those reported from multiple middle-upper Cambrian sections globally (see Section 5.3). Therefore, the $\delta^{34}S_{CAS}$ profile in the present study is inferred to represent a well-preserved primary marine isotopic record.

5.2. Oceanic redox conditions during the SPICE

5.2.1. Redox conditions in study sections

Redox changes on the Jiangnan Slope during the SPICE can be evaluated using elemental proxies (i.e., U_{EF}, Mo_{EF}, and C_{org}/P). Uptake of U commences under suboxic conditions (i.e., around the Fe(III)/Fe(II) redox threshold), whereas uptake of Mo requires euxinic conditions (i.e., presence of aqueous hydrogen sulfide) (Algeo and Li, 2020). Mo-U enrichment can be used to roughly assess bottomwater redox conditions, with U_{EF} of <3, ~3-10, and >10 and Mo_{EF} of <5, ~5-50, and >50 indicative of oxic, suboxic, and euxinic environments, respectively (Algeo and Tribovillard, 2009; Scott and Lyons, 2012). However, the threshold values of Mo_{EF} and U_{EF} are likely to be formation-specific and may vary between depositional systems due to differing uptake pathways (Algeo and Liu, 2020). C_{org}/P ratios are especially useful for redox assessments in carbonate facies (in which low organic content can limit trace-metal uptake), with values of <50, ~50-100, and >100 indicative of oxic, suboxic, and anoxic environments, respectively (Algeo and Ingall, 2007). The P in the study units was originally deposited in association with organic matter and/or Fe-(oxyhydr)oxides rather than carbonate minerals, and it was thus sensitive to redox changes, as shown by positive correlations with TOC and Fe_2O_3, and negative correlations with CaO (see Supplemental Fig. S3).

In the study sections, U_{EF} and Mo_{EF} values are mostly low (<10), indicating that oxic to mildly suboxic conditions prevailed throughout the SPICE event (Figs. 5-7). At Wangcun, U_{EF} and Mo_{EF} peaks are found mainly in samples with low Al content, suggesting that they are artifacts of using a small denominator in the EF calculation. At Duibian A, a shift to moderately reducing (i.e., suboxic) conditions during the Rising SPICE (Unit III) is documented by high U_{EF} (to 5-10) combined with low Mo_{EF} (~1) for samples with Al_2O_3 > 1%, obviating the possibility of an artifact associated with low Al content. A U_{EF} vs. Mo_{EF} crossplot shows that most samples plot in the oxic field, except for a few close to the suboxic field (Fig. 8A-C). C_{org}/P ratios are mostly <30, which strongly supports oxic conditions, with slightly higher values (to ~50) only within Unit III, consistent with somewhat more reducing (e.g., suboxic) conditions during the Rising SPICE (Figs. 5F, 8D). At Duibian, the Mo_{EF} and C_{org}/P proxies covary positively (r = +0.62, n = 69, $p(\alpha) < 0.05$) but lack a significant relationship to U_{EF} (r = –0.01, n = 69, $p(\alpha) > 0.05$, r = –0.20, n = 31, $p(\alpha) > 0.05$, respectively). We regard Mo_{EF} and C_{org}/P as the more reliable redox proxies given the mutual consistency of their secular patterns and the fact that they indicate more reducing conditions at the peak of the SPICE, as expected for an event marked by enhanced marine productivity (Zhou et al., 2015). The pattern of declining U_{EF} during the mid-SPICE may have some other cause, e.g., drawdown of global seawater U concentrations due to expansion of oxygen minimum zones (OMZs) (cf. Hetzel et al., 2009).

The pattern of secular variation in regional seawater redox conditions reconstructed in our study is independently supported by paired CAS and pyrite sulfur isotope (i.e., $\delta^{34}S_{CAS}$ and $\delta^{34}S_{pyrite}$) analyses. The $\Delta^{34}S_{CAS\text{-}pyrite}$ values of both shallow- and deep-water sections from Laurentia and Gondwana are consistently high (~20-40 ‰) in the late Guzhangian, with a decrease to a minimum (~−20 to 0 ‰) in the middle Paibian, followed by a rebound to high values (~20-40 ‰) in the early Jiangshanian (Gill et al., 2011) (Fig. 9D). This pattern is consistent with a strong reduction of the seawater sulfate pool during the Rising SPICE, probably as a result of large-scale pyrite burial and increased amounts of free H_2S in the water column (Algeo et al., 2015), reflecting local expansion of shelf anoxia during the late Guzhangian to the middle Paibian (this study).

5.2.2. Redox conditions in global ocean

The SPICE interval was marked by rising oxygen levels in both the atmosphere and oceans (Zhang et al., 2022). Atmospheric oxygen levels (pO_2) are variously estimated to have risen from ~5 to 10% (Krause et al., 2018) or from ~15 to 25% (Saltzman et al., 2011). This oxygenation event was driven by massive burial of organic matter, as revealed by a global rise in $\delta^{13}C_{carb}$ (Gill et al., 2011), leading to falling atmospheric pCO_2 and climatic cooling. Climatic cooling generally steepens the equator-to-pole temperature gradient (Barron et al., 1995) and invigorates oceanic circulation (Cai and Chu, 1998), mainly through intensification of zonal winds rather than oceanic temperature contrasts (Wunsch, 2002; Huybers and Wunsch, 2010). In the middle-late Cambrian, a cooler climate promoted global-ocean circulation and deep-ocean ventilation during the Rising

SPICE (as revealed by a positive shift in carbonate $\delta^{238}U$; Dahl et al., 2014) as well as a concurrent intensification of continent-margin upwelling (Stouffer et al., 2006). Changes in upwelling intensity were focused along specific continental margins, leading to locally elevated productivity and organic carbon sinking fluxes and, thus, expanded oxygen minimum zones (OMZs), despite a general improvement in deep-ocean ventilation. Thus, global-ocean redox changes during the SPICE event were spatially variable, depending on proximity to paleo-upwelling zones.

Comparison of redox proxy data from the study sections in South China with those for the globally distributed auxiliary sections (Fig. 1A) demonstrates a systematic pattern of environmental redox variation during the SPICE event. The Pre-SPICE to Early SPICE intervals are marked by weaker organic matter burial (thus lower $\delta^{13}C_{carb}$ values) and consequently higher atmospheric pCO_2 (thus warmer climate), which led to weakened global-ocean circulation and depressed marine productivity (cf. Stouffer et al., 2006). This change resulted in expanded global-ocean hypoxia (e.g., a negative shift in $\delta^{238}U$; Dahl et al., 2014), while OMZs on shelf margins contracted (due to low productivity), resulting in mostly oxic conditions on the lower slope (this study) and a reduction in euxinia (as revealed by decreased enrichments of Mo, U and V) on the upper slope (Gill et al., 2021). A major redox transition occurred during the Rising SPICE, when massive organic matter burial (thus higher $\delta^{13}C_{carb}$ values) resulted in declining atmospheric pCO_2 and rising O_2 (Saltzman et al., 2011; Krause et al., 2018). Concurrently, climatic cooling due to lower pCO_2 led to improved global-ocean ventilation and oxygenation (i.e., first-order positive shifts in $\delta^{238}U$; Dahl et al., 2014), while elevated marine productivity led to an expansion of OMZs (i.e., locally more hypoxic conditions in lower slope settings; this study). Ocean-redox conditions changed again during the Falling SPICE, marked by a contraction of OMZs in the late Paibian to early Jiangshanian that resulted in a return of oxic conditions to deep slope facies (e.g., Duibian, this study). This development was probably in response to reduced marine productivity, as recorded by declining $\delta^{13}C$-$\delta^{34}S$ of the Falling SPICE interval.

Despite commonalities in temporal patterns of redox variation, the study and auxiliary sections exhibit regionally unique features that may have been due to differences in water depth, watermass restriction, or regional oceanic circulation (see Supplemental file for facies data and water-depth interpretations). Compared to the largely oxic conditions observed in South China, some localities exhibit more intense seawater de-oxygenation. For example, local redox proxy data (e.g., Fe speciation) for the Andrarum no. 3 core (Alum Shale, Sweden) record dominantly euxinic conditions during the Pre-SPICE, followed by a shift toward less reducing conditions (ferruginous) close to the peak of the SPICE, and a return to euxinic conditions during the Falling and Post-SPICE intervals (Gill et al., 2011, 2021; Dahl et al., 2013). This pattern was punctuated by short-term (millennial-scale) dysoxic episodes, as inferred from sedimentological and ichnological data (Egenhoff et al., 2015). The generally more reducing conditions of the Alum Shale may have been related to stagnation of watermass circulation on the Baltic Craton during the Cambrian eustatic highstand (Thickpenny, 1987; Høyberget and Bruton, 2008). Moreover, OMZ

545 expansion during the Rising SPICE did not cause enrichments of trace metals (e.g., Mo, U, and V)
546 in the Alum Shale (Gill et al., 2021), which is consistent with either regional watermass restriction
547 (cf. Algeo and Maynard, 2008) or a general drawdown of trace metals in the global ocean linked
548 to expanded anoxia in the Early SPICE interval (cf. Dahl et al., 2014, 2019). A global-ocean redox
549 proxy record (i.e., carbonate $\delta^{238}U$) has been generated only for the Mount Whelan core (Australia;
550 Dahl et al., 2014). It shows an intensification of global-oceanic hypoxia during the Pre-SPICE to
551 early Rising SPICE, with a shift towards more oxic conditions in the late Rising SPICE, before a
552 probable re-expansion of anoxic facies during the Falling SPICE, although aspects of these
553 interpretations are somewhat uncertain owing to the sparsity and unequal temporal distribution of
554 the $\delta^{238}U$ data.
555
556 *5.3. Global carbon-sulfur cycle changes during the SPICE*
557 The marine carbon and sulfur cycles are commonly coupled through biochemical processes
558 such as photosynthesis and microbial sulfate reduction (Jorgensen, 1982; Mazumdar et al., 2012;
559 Antler et al., 2013). Major fractionations of carbon and sulfur isotopes are associated with the
560 production of organic matter from dissolved inorganic carbon (DIC) and pyrite from sulfate
561 (Bottrell and Newton, 2006). Owing to the long residence times of DIC and sulfate in the ocean
562 (~100 kyr and ~13 Myr, respectively; Claypool et al., 1980; Zeebe and Wolf-Gladrow, 2001), their
563 isotopic compositions in seawater generally reflect changes in the burial fluxes of organic matter
564 and pyrite.
565 During the Early and Rising SPICE, the carbon and sulfur isotopic profiles show general
566 first-order positive excursions. At Wangcun and Duibian A, the late Guzhangian to middle Paibian
567 interval (i.e., Units II to III) is characterized by roughly simultaneous positive excursions of
568 $\delta^{34}S_{CAS}$ (~+35 ‰ to ~+50 ‰ and ~+30 ‰ to ~+50 ‰, respectively), and $\delta^{13}C_{carb}$ (~0 ‰ to ~+4 ‰
569 and ~+1 ‰ to ~+4 ‰, respectively). At Wangcun, $\delta^{34}S_{CAS}$ is positive correlated (r = +0.59, n = 9,
570 $p(\alpha) \sim 0.05$) to $\delta^{13}C_{carb}$ during the Early SPICE, while no relationship (r = –0.43, n = 5, $p(\alpha) >$
571 0.05) exists during the Rising SPICE (Fig. 2C-D). At Duibian A, a rise of $\delta^{34}S_{CAS}$ (~+30 ‰ to
572 ~+45 ‰) corresponds to nearly no changes of $\delta^{13}C_{carb}$ (~+1 ‰) during the Early SPICE, while a
573 positive correlation is marginally statistically significant (r = +0.67, n = 7, $p(\alpha) \sim 0.05$) during the
574 Rising SPICE (Fig. 3C-D). The first-order positive correlation between $\delta^{34}S_{CAS}$ and $\delta^{13}C_{carb}$ during
575 the Early and Rising SPICE suggests coupling of the global marine carbon and sulfur cycles,
576 presumably due to co-burial of organic matter and pyrite and a small reservoir of marine sulfate,
577 driven by elevated marine productivity and expanded shelf/slope hypoxia (Dahl et al., 2014;
578 Zhang et al., 2022; this study).
579 During the Falling SPICE, the carbon and sulfur isotopic profiles show negative excursions
580 and intermittent coupling. The late Paibian-early Jiangshanian interval (i.e., Falling SPICE, Unit
581 IV) is characterized by simultaneous shifts toward lower $\delta^{13}C_{carb}$ and $\delta^{34}S_{CAS}$ values, declining to
582 minima of ~+1 ‰ and ~+15 to +20 ‰, respectively. The correlations are significant for $\delta^{34}S_{CAS}$ vs.
583 $\delta^{13}C_{carb}$ at Wangcun (r = +0.63, n = 7, $p(\alpha) \sim 0.05$) and Duibian A (r = +0.56, n = 14, $p(\alpha) < 0.05$),

but not at Duibian B (r = +0.17, n = 38, $p(\alpha) > 0.10$) (Figs. 2C-D, 3C-D, 4C-D). These differences may exist owing to regional variation in the net burial rates of organic matter and pyrite, but they are not inconsistent with reduced marine productivity in South China during the Falling SPICE.

In contrast to the SPICE, the Pre-SPICE and Post-SPICE intervals in the study sections are characterized by non-synchronous variation in $\delta^{34}S_{CAS}$ and $\delta^{13}C_{carb}$, suggesting a general decoupling of the global marine carbon and sulfur cycles. In detail, the middle Drumian to middle Guzhangian interval (i.e., Pre-SPICE, Unit Ib) exhibits fluctuations in $\delta^{34}S_{CAS}$ (from ~+25 ‰ to ~+35 ‰) that coincided with little change in $\delta^{13}C_{carb}$ (~0 ‰) at Wangcun (Fig. 2C-D). The early Jiangshanian interval (i.e., Post-SPICE, Unit IV) exhibits a shift toward lower $\delta^{13}C_{carb}$ values (~+1 ‰) that is decoupled from $\delta^{34}S_{CAS}$ at Wangcun (r = −0.07, n = 8, $p(\alpha) > 0.10$) and Duibian B (r = +0.44, n = 11, $p(\alpha) > 0.10$) (Figs. 2C-D, 3C-D). Thus, variations in marine productivity and organic carbon and pyrite burial were not sufficiently large in the pre-SPICE and post-SPICE intervals to override other influences on the global marine carbon and sulfur cycles.

All of the auxiliary sections show $\delta^{13}C_{carb}$-$\delta^{34}S_{CAS}$ coupling during the late Guzhangian to earliest Jiangshanian (i.e., Early to Falling SPICE) and decoupling during the early-middle Guzhangian (i.e., Pre-SPICE) and early Jiangshanian (i.e., Post-SPICE), conforming to the general pattern reported here for Wangcun and Duibian. Covariation of $\delta^{13}C_{carb}$ and $\delta^{34}S_{CAS}$ is observed not only in deep-water sections (e.g., TE-1 Texas County Core, Duibian) but also in intermediate-depth (e.g., Mount Whelan Core, Shingle Pass) and shallow-water (e.g., Lawson Cove) sections of Laurentia and Gondwana (Fig. 9). This transregional pattern of carbon-sulfur cycling confirms marine productivity as the main control on coupled $\delta^{13}C_{carb}$-$\delta^{34}S_{CAS}$ variation throughout the SPICE event (cf. Dahl et al., 2014). In contrast, the Pre-SPICE and Post-SPICE intervals were likely associated with a warmer climate, more sluggish oceanic circulation, and lower (and less variable) marine productivity.

5.4. Trilobite biodiversity and its relationship to environmental changes during the SPICE event

5.4.1. Global comparison of trilobite biodiversity

Trilobite biostratigraphic studies from Laurentia resulted in recognition of the EMBE at the end of the Guzhangian Stage and the ESBE in the early Jiangshanian Stage, each of which reportedly exhibits two phases of extinction (Longacre, 1970; Palmer, 1965a, 1965b; Stitt, 1971; Taylor, 2006; Babcock et al., 2017). For the EMBE, the first phase coincided with the base of the Laurentian *Coosella perplexa* Subzone of the latest Guzhangian (i.e., Early SPICE) and was marked by the disappearance of the majority of shallow-water trilobites with no concurrent change in $\delta^{13}C_{carb}$ values (Palmer, 1979; Gerhardt and Gill, 2016). The second phase of the EMBE was less severe and coincided with the uppermost *C. perplexa* Subzone of the Early Paibian (i.e., onset of the Rising SPICE), marked by the disappearance of surviving members of the *C. perplexa* Subzone fauna. Generally, the EMBE is characterized not only by a decline in species diversity but also by a shift to biofacies that have broader environmental distributions as well as extensive immigration of taxa from off-shelf and shelf-margin sites to shelf areas (Westrop and Cuggy,

1999). The ESBE is relatively less studied than the EMBE, but its first and second phases coincided with the lowermost *Ir. major* Zone and the *Taenicephalus* Zone of the early Jiangshanian (i.e., Post-SPICE), respectively. Collectively, these extinctions resulted in a shift in dominance from the Marjumiid Biomere of the Guzhangian to the Pterocephaliid Biomere of the earliest Paibian, and subsequently to the Ptychaspid Biomere of the early Jiangshanian (Palmer, 1984; Saltzman et al., 2000) (Fig. 10). Although biomeres were first recognized from patterns seen in Laurentian trilobite faunas, correlative patterns of diversity changes can now be recognized elsewhere, including in South China (Zhou and Zhen, 2008; Zhang et al., 2021).

The trilobite biodiversity curves generated for the present study are only regionally representative but nonetheless in broad accord with global evolutionary trends during the late Guzhangian. Thus, although the Marjumiid, Pterocephaliid, and Ptychaspid biomeres *sensu stricto* were endemic to Laurentia (e.g., Saltzman et al., 2000), similar and iterative patterns of trilobite evolutionary diversification can be seen in age-equivalent successions in South China (Zhang et al., 2021; this study), making these biomeres *sensu lato* of global significance. In the present study, the first phase of the EMBE is recognizable as a decrease in trilobite range-through species diversity from ~>10 to 1 at Wangcun (i.e., at ~230-270 m) and from ~25 to ~5 at Duibian (i.e., at ~–4 to +1 m), during an interval of nearly constant or slightly positive-shifted $\delta^{13}C_{carb}$ values (i.e., Early SPICE) (Fig. 10A, D). A similar decline in trilobite diversity without a major carbon isotope excursion has been reported from strata in Laurentia that are age-equivalent to the Early SPICE interval (Palmer, 1979, 1984; Gerhardt and Gill, 2016) (Fig. 10E). This observation suggests that the trilobite diversity curves in the present study are globally representative (cf. Zhou and Zhen, 2008; Zhang et al., 2021), and that the EMBE was a widespread event triggered by global environmental changes during the Early SPICE interval.

The newly generated trilobite diversity curves for the Rising SPICE interval at both Wangcun and Duibian are regionally representative (see Zhang et al., 2021). Although a gradual increase in trilobite diversity occurred immediately after the EMBE in Laurentia (Fig. 10E; Palmer, 1984; Rowell and Brady, 1976), our study reveals a trend toward lower diversity at ~1-30 m in Duibian A, coincident with an increase of $\delta^{13}C_{carb}$ and stable $\delta^{34}S_{CAS}$ values during the Rising SPICE, reaching a minimum of one species at the peak of the SPICE (Fig. 10D). A drop in taxonomic diversity during the Rising SPICE was also reported from the Paibi section (which is the GSSP of the base of the Furongian Series and Paibian Stage), ~50 km southwest of Wangcun (Peng et al., 2004; Zhang et al., 2021). However, a recent study from South China inferred approximately constant trilobite diversity during the Rising SPICE, before a decline during the Falling SPICE (Zhang et al., 2021).

The trilobite biodiversity curves from the present study are in accord with documented evolutionary trends for the Jiangshanian of South China (Zhou and Zhen, 2008; Zhang et al., 2021), which may be representative of contemporaneous global patterns. Trilobite species diversity remained at a higher level through the end of the SPICE, before declining during the ESBE at the transition to the Post-SPICE interval (Palmer, 1979, 1984; Zhou and Zhen, 2008; this

study). Biodiversity changes in South China are comparable to those reported from correlative units in Laurentia (Fig. 10D-E), although, as with the EMBE, the existence of two separate extinction pulses during the ESBE has not been recognized in the present study sections.

Proposed triggers for the EMBE include cooling climate/seawater (e.g., climatic cooling, rise of permanent thermocline, and upwelling of cool nutrient-rich waters) (Öpik, 1966; Lochman-Balk, 1970; Stitt, 1975; Perfetta et al., 1999; Elrick et al., 2011), and seawater anoxia and/or euxinia (Saltzman et al., 1998; Hurtgen et al., 2009; Gill et al., 2011; Dahl et al., 2014). In contrast, the environmental controls on the ESBE have received little consideration to date. Below, we consider possible environmental controls on the EMBE and ESBE, based on a combination of previous studies and our new paleontological and geochemical data.

5.4.2. End-Marjuman Biomere Extinction (EMBE)

The cause of the extinction of the Marjumiid Biomere (*sensu lato*) and the spread of the Pterocephaliid Biomere (*sensu lato*) over shelf areas during the Early SPICE has long been debated. Early work focused on differences in the preferred habitats of these two biomeres (Palmer, 1984; Pratt, 1992). The fauna of the Marjumiid Biomere mostly occupied shallow-water sandstone and siltstone facies close to paleo-shorelines, resulting in relatively high degrees of endemism. In contrast, the fauna of the Pterocephaliid Biomere was better represented in deeper-water, shale-rich facies beneath the oceanic thermocline, allowing it to migrate globally and develop into a eurytopic assemblage (Pratt, 1992). More recent work has focused on the role of temperature change, with climatic cooling, a rise of the permanent thermocline, and/or upwelling of deep waters being proposed as the trigger for the EMBE (Palmer, 1984; Saltzman et al., 2000; Elrick et al., 2011). Whereas the Marjumiid Biomere favored warmer waters, the Pterocephaliid Biomere, and especially its agnostoid elements and olenimorphic morphotypes, preferred cooler, deeper waters (Fortey and Owens, 1990), although one of its members, the genus *Erixanium*, had a narrow latitudinal range centered on the paleo-Equator (Lu and Lin, 1989; Stitt et al., 1994; Zhou and Zhen, 2008), suggesting a preference for warmer temperatures (Hughes, 2000). At Duibian, representatives of the Pterocephaliid Biomere comprise a low-diversity fauna dominated by proceratopygine and iwayaspine species (Lu and Lin, 1989; Hughes and Rushton, 1990; Peng et al. 2012) that may have been especially tolerant of challenging or variable environmental conditions linked to oxygen stress (cf. Zhang et al., 2021). This fauna yielded to the Ptychaspiid Biomere, which was characterized by a decline in endemic species and an increase in more cosmopolitan elements (Cook and Taylor, 1975; Żylińska, 2001, 2002; Álvaro et al., 2013). Taxa appearing immediately after the ESBE include both the widespread and arguably pelagic genus *Irvingella* (Fortey, 1985), which was adept at crossing open ocean basins, and the more typical "ptychopariid" *Maladioidella*, which was restricted to shallow-shelf settings along the margin of Gondwana (Rushton and Hughes, 1996) but spanned an unusually wide range of paleolatitudes (Hughes, 2000). Such widespread occurrence along the Gondwanan margin may attest to a reduced latitudinal temperature gradient following the ESBE, possibly associated with

global warming. The biotic succession in the present study sections is thus consistent with cooling in conjunction with the EMBE followed by warming in association with the ESBE.

The biotic extinctions during the Early SPICE may have been analogous to the extinction events at the onset and termination of the Hirnantian Glaciation of the Late Ordovician, about 50 Myr later (Algeo et al., 2016). The <1-Myr-long Hirnantian Glaciation was marked by a ~5 °C decline of global temperatures (Trotter et al., 2008; Finnegan et al., 2011), a ~70-150 m sea-level fall (Brenchley et al., 2003; Finnegan et al., 2011), and a ~4-6 ‰ positive $\delta^{13}C$ excursion (i.e., the Hirnantian carbon isotope excursion or HICE, Bergström et al., 2006). An extinction of warm-water faunas at the onset of this glacial episode (Barash, 2014) and its replacement by the cool-water-adapted *Hirnantia* Fauna (Zhan et al., 2010; Rasmussen and Harper, 2011) were possibly analogous to the transition from the warm-water Marjumiid Biomere to the cool-water Pterocephaliid Biomere during the Early SPICE (Palmer, 1984; Pratt, 1992).

The role of temperature change as a control on trilobite biomeres during the middle-late Cambrian has been inadequately tested to date using oxygen-isotope data. Phosphatic brachiopod $\delta^{18}O$ from western Laurentia provided evidence of a climate cooling event during the Pre-SPICE, followed by climate warming during the Rising SPICE (Elrick et al., 2011). However, this pattern is likely to represent only a local signal linked to shallowing of a tropical shelf as a result of global sea-level fall (Fig. 10F), shifting the local watermass from the cooler thermocline into the warmer surface layer of the ocean during the SPICE. The EMBE was followed by the rise of the cool-water Pterocephaliid Biomere fauna in western Laurentia (Stitt, 1975; Rowell and Brady, 1976; Palmer, 1984), which is inconsistent with the general climatic warming inferred by Elrick et al. (2011). However, global climate cooling is likely to have prevailed during the SPICE, as evidenced by sedimentological, stratigraphic, and geochemical records (e.g., greater burial sequestration of organic matter, and thus a reduced greenhouse effect) (Saltzman, 2005; Cherns and Wheeley, 2009; Sørensen et al., 2020) (Fig. 10I).

Redox changes are likely to have contributed to trilobite biomere turnovers, although the extinction of the Marjuman Biomere during the latter part of the Early SPICE lagged a major negative shift in carbonate $\delta^{238}U$ during its earlier part (Dahl et al., 2014; note: some uncertainty linked to limited fossil data from Whelan core), suggesting that transient expansion of global-ocean hypoxia was not the proximate cause of the EMBE. Rather, the EMBE may have been due to the impact of global-ocean circulation changes on regional redox conditions. Global climatic cooling is likely to have led to an expansion of seawater hypoxia on shelf margins subject to upwelling, where nutrient-rich deepwaters enhanced regional productivity and organic carbon sinking fluxes, producing locally more reducing conditions (cf. Whitney et al., 2005; Stouffer et al., 2006). This hypothesis is consistent with a concurrent improvement in global-ocean ventilation during the Early SPICE and Rising SPICE, as evidenced by first-order positive shifts of carbonate $\delta^{238}U$ (Dahl et al., 2014). The present study provides evidence of OMZ expansion as shown by a transition from oxic to suboxic waters on the Jiangnan Slope of South China during the Rising SPICE (Fig. 10C). This redox change is likely to have placed outer-shelf trilobite communities

under stress despite generally improved ventilation of the global ocean. The extinction of indigenous cool-water trilobites belonging to the early Paibian Pterocephaliid Biomere in deep-slope settings supports our inference of OMZ expansion and increased shelf anoxia as the principal control on the EMBE and the subsequent reduced diversity of the Pterocephaliid Biomere (cf. Pratt, 1992), as does the nature of the trilobites that dominate the Paibian fauna (see above). During the latter part of the Falling SPICE, contraction of OMZs on shelf margins permitted local increases in the abundance and diversity of the Pterocephaliid Biomere fauna *sensu lato* prior to the ESBE (Fig. 10D).

5.4.3. End-Steptoean Biomere Extinction (ESBE)

The causes of the ESBE remain uncertain. Given that the ESBE occurred at the end of a period of global carbon cycle instability, this biotic event is likely to have been related to the attenuation of environmental disturbances associated with the carbon cycle. The ESBE was probably related to global climate change but evidence for this is presently scant. Bioapatite oxygen isotopes suggest that in Laurentia, the Falling and Post-SPICE episodes corresponded to a cooling climate (Elrick et al., 2011), although cooling may have been due to local water-column deepening as a result of global warming and continental ice mass decay. Global climate change during the ESBE has not been studied to date. If the ESBE is analogous to the extinction of the *Hirnantia* Fauna at the termination of the Hirnantian Glaciation, then it may also have been associated with global climatic warming (Fig. 10I). However, environmental factors controlling the ESBE were probably not simply the opposite of those influencing the EMBE (e.g., climate warming as opposed to earlier climate cooling), because there are cosmopolitan taxa among both the latest Paibian and early Jiangshanian biomeres (e.g., *Hedinaspis, Irvingella*, and *Maladioidella* at Duibian; Peng et al., 2012).

The spatial scale of seawater redox changes during the ESBE requires consideration. As oxic seawater conditions persisted during this time interval throughout the study area, local redox changes cannot explain this extinction event (Fig. 10C). Widespread seawater anoxia may have developed in the global ocean during this interval, as indicated by rapid increases in $\delta^{34}S_{CAS}$ and $\Delta^{34}S_{CAS\text{-}pyrite}$ in both South China and Laurentia (Fig. 9). However, the geographic extent of oceanic redox changes remains to be tested via a proxy suitable for addressing global trends (e.g., carbonate U isotopes).

6. Conclusions

Paired $\delta^{13}C_{carb}$-$\delta^{34}S_{CAS}$ profiles and trilobite species diversity curves spanning the lower Drumian to lower Jiangshanian were generated for a shallow-water succession at Wangcun and a deep-water succession at Duibian, located on the Jiangnan Slope in South China. Enrichment factors for U and Mo, along with C_{org}/P ratios, suggest mostly oxic conditions in the study sections during the SPICE event, except hypoxic (i.e., suboxic) seawater conditions from the earliest Paibian to the middle Paibian (i.e., Rising SPICE) at Duibian. $\delta^{13}C_{carb}$ was tightly coupled with

779 $\delta^{34}S_{CAS}$ during the late Guzhangian to late Paibian, demonstrating first-order control of
780 contemporaneous environmental changes by the marine carbon cycle. Local $\delta^{13}C_{carb}$ trends mirror
781 positive excursions of ~3 ‰ found globally during the Rising SPICE, which were driven by
782 elevated global marine productivity and enhanced burial of organic matter. The major positive
783 excursion in $\delta^{34}S_{CAS}$ started earlier than that of $\delta^{13}C_{carb}$ during the Early SPICE, and $\delta^{34}S_{CAS}$
784 remained stable during the Rising SPICE before declining during the Falling SPICE. The Falling
785 SPICE was characterized by diminished global marine productivity, resulting in reduced co-burial
786 of organic matter and pyrite. In order to investigate the global marine carbon-sulfur cycles during
787 the SPICE event, we further compiled $\delta^{13}C_{carb}$-$\delta^{34}S_{CAS}$ variations in four shallow- to deep-water
788 successions on the slope/continental margin of Laurentia and Gondwana. The relationship
789 between $\delta^{13}C_{carb}$ and $\delta^{34}S_{CAS}$ in these settings is similar to that at Wangcun and Duibian,
790 suggesting globally consistent patterns of carbon-sulfur cycling during the SPICE event.
791 The local trilobite species diversity curves are comparable to those from Laurentia, showing a
792 major decline in biodiversity during the End-Marjuman Biomere Extinction (EMBE) in the Early
793 SPICE, as well as the End-Steptoean Biomere Extinction (ESBE) in the Post-SPICE. Therefore,
794 the SPICE event should be extended downwards to include the Early SPICE interval of the late
795 Guzhangian Stage, in a manner that more clearly links the EMBE to the SPICE. We further
796 evaluated effects of climate change, global and local seawater redox conditions on these biotic
797 extinctions, and propose that expansion of seawater hypoxia on shelf margins as a result of global
798 climate cooling, invigorated global ocean circulation, and intensified continent-margin upwelling
799 may have directly contributed to the extinction of the trilobite fauna of the Marjumiid Biomere
800 during the Early SPICE, and the attenuation of those environmental changes during the Falling
801 SPICE set the stage for the subsequent extinction of the Pterocephaliid Biomere.
802
803 **Acknowledgments**
804 We thank Science Editors Brad Singer and Rob Strachan for handling this manuscript, and
805 we thank Associate Editor Bradley D. Cramer and two anonymous reviewers for their constructive
806 comments. We thank Ziheng Li, Guoxiong Ou and Ziliang Wan for their help in the field and
807 laboratory. This study is supported by NSFC grants (42073073, 92055212，41977264, 41930322,
808 41825019, 41803011, 41821001, 42130208), the Fundamental Research Funds for the Central
809 Universities, China University of Geosciences–Wuhan (CUGCJ1815, CUGQYZX1728), and the
810 MOST Special Fund (MSF-GPMR2022-7) of the State Key Laboratory of Geological Processes
811 and Mineral Resources, China University of Geosciences, Wuhan. TWD thanks the Carlsberg
812 Foundation (CF16-0876) for financial support. This is a contribution to IGCP668, and N.C.H.
813 acknowledges NSF EAR-1849963.
814
815 **References**
816 Algeo, T.J., and Ingall, E., 2007, Sedimentary C_{org}:P ratios, paleocean ventilation, and Phanerozoic
817 atmospheric pO_2: Palaeogeogr. Palaeoclimatol. Palaeoecol., v. 256, p. 130–155.

818 Algeo, T.J., and Li, C., 2020, Redox classification and calibration of redox thresholds in
819 sedimentary systems: Geochimica et Cosmochimica Acta, v. 287, p. 8–26.
820 Algeo, T.J., and Liu, J.S., 2020, A re-assessment of elemental proxies for paleoredox analysis:
821 Chem. Geol., v. 540, p. 119549.
822 Algeo, T.J., and Maynard, J.B., 2008, Trace-metal covariation as a guide to water-mass conditions
823 in ancient anoxic marine environments: Geosphere, v. 4, p. 872-887.
824 Algeo T.J., and Tribovillard N., 2009, Environmental analysis of paleoceanographic systems based
825 on molybdenum–uranium covariation: Chem. Geol., v. 268, p. 211–225.
826 Algeo, T.J., Rowe, H., Hower, J. C., Schwark, L., Herrmann, A., and Heckel, P., 2008, Changes in
827 ocean denitrification during Late Carboniferous glacial–interglacial cycles: Nature
828 Geoscience, v. 1, p. 709–714.
829 Algeo, T.J., Luo, G.M., Song, H.Y., Lyons, T.W., and Canfield, D.E., 2015, Reconstruction of
830 secular variation in seawater sulfate concentrations: Biogeosciences, v. 12, p. 2131-2151.
831 Algeo, T.J., Marenco, P.J., and Saltzman, M.R., 2016, Co-evolution of oceans, climate, and the
832 biosphere during the 'Ordovician Revolution': a review: Palaeogeography, Palaeoclimatology,
833 Palaeoecology, v. 458, p. 1–11.
834 Al-Husseini, M.I., 2017, Late Cambrian SPICE and Ice. 12 pp. www.orbitalscale.com.
835 Álvaro, J.J., Ahlberg, P., Babcock, L.E., Bordonaro, O. L., Choi, D.K., Cooper, R.A., Ergaliev,
836 G., Kh., Gapp, I.., Ghobadi Pour, M., Hughes, N.C., Jago, J.B., Korovnikov, I., Laurie, J.R.,
837 Lieberman, B.S., Paterson, J.R., Pegel, T.V., Popov, L.E., Rushton, A.W.A., Sukhov, S.S.,
838 Tortello, M.F., Zhou, Z.-Y., and Żyli ń ska, A., 2013, Global Cambrian trilobite
839 palaeobiogeography assessed using parsimony analysis of endemicity, *in* Harper, D.A.T., and
840 Servais, T., eds., Early Palaeozoic Palaeobiogeography and Palaeogeography, Geological
841 Society of London, Memoir 38, p. 273–296.
842 Anderson, R.F., Fleisher, M.Q., and LeHuray, A.P., 1989, Concentration, oxidation state, and
843 particulate flux of uranium in the Black Sea: Geochimica et Cosmochimica Acta, v. 53, p.
844 2215–2224.
845 Antler, G., Turchyn, A.V., Rennie, V., Herut, B., and Sivan, O., 2013, Coupled sulfur and oxygen
846 isotope insight into bacterial sulfate reduction in the natural environment: Geochimica et
847 Cosmochimica Acta, v. 118, p. 98–117.
848 Babcock, L.E., Peng, S., and Ahlberg, P., 2017, Cambrian trilobite biostratigraphy and its role in
849 developing an integrated history of the Earth system: Lethaia, v. 50, p. 381–399.
850 Baker, J.L., 2010, Carbon isotopic fractionation across a late Cambrian carbonate platform: a
851 regional response to the SPICE event as recorded in the Great Basin, United States [M.S.
852 thesis]: Las Vegas, University of Nevada, 681 pp.
853 Barash, M.S., 2014, Mass extinction of the marine biota at the Ordovician-Silurian transition due
854 to environmental changes: Oceanology, v. 54, p. 780–787.
855 Barron, E.J., Fawcett, P.J., Peterson, W.H., Pollard, D. and Thompson, S.L., 1995, A "simulation"
856 of mid - Cretaceous climate: Paleoceanography, v. 10, p. 953-962.
857 Bergström, S.M., Saltzman, M.M., and Schmitz, B., 2006, First record of the Hirnantian (Upper

858 Ordovician) $\delta^{13}C$ excursion in the North American midcontinent and its regional implications:
859 Geological Magazine, v. 143, p. 657–678.
860 Bottrell, S.H., and Newton, R.J., 2006, Reconstruction of changes in global sulfur cycling from
861 marine sulfate isotopes: Earth Science Reviews, v. 75, p. 59–83.
862 Brand, U., 2004, Carbon, oxygen and strontium isotopes in Paleozoic carbonate components: an
863 evaluation of original seawater-chemistry proxies: Chem. Geol., v. 204, p. 23–44.
864 Brenchley, P.J., Carden, G.A., Hints, L., Kaljo, D., Marshall, J.D., Martma, T., and Nõlvak, J.,
865 2003, High-resolution stable isotope stratigraphy of Upper Ordovician sequences: constraints
866 on the timing of bioevents and environmental changes associated with mass extinction and
867 glaciation: Geological Society of America Bulletin, v. 115, p. 89–104.
868 Cai, W., and Chu, P.C., 1998, Oceanic responses to gradual transitions of equator–to–pole
869 temperature–gradients: Quarterly Journal of the Royal Meteorological Society, v. 124, p.
870 2817–2828.
871 Cherns, L., and Wheeley, J.R., 2009, Early Palaeozoic cooling events: Peri-Gondwana and beyond.
872 In: Bassett, M.G. (ed.) Early Palaeozoic Peri-Gondwana Terranes, New Insights from
873 Tectonics and Biogeography: Geological Society of London, Special Publication, v. 325, p.
874 257–278.
875 Claypool, G.E., Holser, W.T., Kaplan, I.R., Sakai, H., and Zak, I., 1980, The age curves for sulfur
876 and oxygen isotopes in marine sulfate and their mutual interpretation: Chemical Geology, v.
877 28, p. 199–260.
878 Cook, H.E., and Taylor, M.E., 1975, Early Paleozoic continental margin sedimentation, trilobite
879 biofacies, and the thermocline, western United States: Geology, v. 3, p. 559–562.
880 Dahl, T.W., Boyle, R.A., Canfield, D.E., Connelly, J.N., Gill, B.C., Lenton, T.M., and Bizzarro, M.,
881 2014, Uranium isotopes distinguish two geochemically distinct stages during the later
882 Cambrian SPICE event: Earth Planet. Sci. Lett., v. 401, p. 313–326.
883 Dahl, T.W., Ruhl, M., Hammarlund, E.U., Canfield, D.E., Rosing, M.T., Bjerrum, C.J., 2013,
884 Tracing euxinia by molybdenum concentrations in sediments using handheld X-ray
885 fluorescence spectroscopy (HHXRF): Chemical Geology, v. 360, p. 241-251.
886 Dahl, T.W., Siggaard-Andersen, M.L., Schovsbo, N.H., Persson, D.O., Husted, S., Hougård, I.W.,
887 Dickson, A.J., and Nielsen, A.T., 2019, Brief oxygenation events in locally anoxic oceans
888 during the Cambrian solves the animal breathing paradox: Scientific Reports, v. 9, p. 1–9.
889 Dronov, A., and Popov, L.E., 2004, Traces of frost action in the Obolus-Sand: The evidence for
890 sub-glacial climate in the mid-Cambrian to early Ordovician (Tremadocian) of the east Baltic
891 (abstract). In: Munnecke, A., Servais, T., Schulbert, C. (eds) Early Palaeozoic
892 Palaeogeography and Palaeoclimate: Erlanger Geologische Abhandlungen, v. 5, 32 pp.
893 Edwards, C.T., Fike, D.A., and Saltzman, M.R., 2019, Testing carbonate-associated sulfate (CAS)
894 extraction methods for sulfur isotope stratigraphy: A case study of a Lower–Middle
895 Ordovician carbonate succession, Shingle Pass, Nevada, USA: Chemical Geology, v. 529,
896 119297.

Egenhoff, S.O., Fishman, N.S., Ahlberg, P., Maletz, J., Jackson, A., Kolte, K., Lowers, H., Mackie, J., Newby, W., and Petrowsky, M., 2015, Sedimentology of SPICE (Steptoean positive carbon isotope excursion): a high-resolution trace fossil and microfabric analysis of the middle to late Cambrian Alum Shale Formation, southern Sweden. In: Larsen, D., Egenhoff, S.O., Fishman, N.S. (eds.), Paying Attention to Mudrocks: Priceless!: Geol. Soc. Am. Spec. Pap.. v. 515, p. 87–102.

Elrick, M., Rieboldt, S., Saltzman, M., and McKay, R.M., 2011, Oxygen-isotope trends and seawater temperature changes across the Late Cambrian Steptoean positive carbon-isotope excursion (SPICE event): Geology, v. 39, p. 987–990.

Feng, Z.Z., Peng, Y.M., Jin, Z.K., and Bao, Z.D., 2002, Lithofacies Palaeogeography of the Middle Cambrian. China Journal of Palaeogeography, v. 4, p. 1–11.

Finnegan, S., Bergmann, K., Eiler, J.M., Jones, D.S., Fike, D.A., Eisenman, I., Hughes, N.C., Tripati, A.K., and Fischer, W.W., 2011, The magnitude and duration of Late Ordovician-Early Silurian glaciation: Science, v. 331, p. 903–906.

Fortey, R.A., 1985, Pelagic trilobites as an example of deducting life habits in extinct arthropods: Transactions of the Royal Society of Edinburgh, v. 76, p. 219-230.

Fortey, R.A., and Owens, R.M., 1990. Evolutionary radiations in the Trilobita: In Major evolutionary radiations, p. 139-164.

Gerhardt, A.M., and Gill, B.C., 2016, Elucidating the relationship between the later Cambrian end-Marjuman extinctions and SPICE Event: Palaeogeography Palaeoclimatology Palaeoecology, v. 461, p. 362–373.

Gill, B.C., Lyons, T.W., and Saltzman, M.R., 2007, Parallel, high-resolution carbon and sulfur isotope records of the evolving Paleozoic marine sulfur reservoir: Palaeogeogr. Palaeoclimatol. Palaeoecol., v. 256, p. 156–173.

Gill, B.C., Lyons, T.W., Young, S.A., Kump, L.R., Knoll, A.H., and Saltzman, M.R., 2011, Geochemical evidence for widespread euxinia in the later Cambrian ocean: Nature, v. 469, p. 80–83.

Gill, B.C., Dahl, T.W., Hammarlund, E.U., LeRoy, M.A., Gordon, G.W., Canfield, D.E., Anbar, A.D., and Lyons, T.W., 2021, Redox dynamics of later Cambrian oceans: Palaeogeography, Palaeoclimatology, Palaeoecology, v. 581, 110623.

Hammer, Ø., and Svensen, H.H., 2017, Biostratigraphy and carbon and nitrogen geochemistry of the SPICE event in Cambrian low-grade metamorphic black shale, Southern Norway: Palaeogeogr. Palaeoclimatol. Palaeoecol., v. 468, p. 216–227.

Hetzel, A., Böttcher, M.E., Wortmann, U.G., and Brumsack, H.J., 2009, Paleo-redox conditions during OAE 2 reflected in Demerara Rise sediment geochemistry (ODP Leg 207): Palaeogeography, Palaeoclimatology, Palaeoecology, v. 273, p. 302–328.

Høyberget, M., and Bruton, D.L., 2008, Middle Cambrian trilobites of the suborders Agnostina and Eodiscina from the Oslo Region, Norway: Palaeontogr. Abt. A, v. 286, p. 1–87.

935 Hughes, N. C., 2000, Ecologic evolution of Cambrian trilobites. pp. 370-403. *In* Zhuravlev, A.Y. &
936 Riding, R., Eds. The Ecology of the Cambrian Radiation: Columbia University Press, New
937 York.
938 Hughes, N.C., and Rushton, A.A., 1990, Computer-aided restoration of a Late Cambrian
939 ceratopygid trilobite from Wales, and its phylogenetic implications: Palaeontology, v. 33, p.
940 429–445.
941 Hurtgen, M.T., Pruss, S.B., and Knoll, A.H., 2009, Evaluating the relationship between the carbon
942 and sulfur cycles in the later Cambrian ocean: an example from the Port au Port Group,
943 western Newfoundland, Canada: Earth Planet. Sci. Lett., v. 281, p. 288–297.
944 Huybers, P., and Wunsch, C., 2010, Paleophysical oceanography with an emphasis on transport
945 rates: Annual Review of Marine Science, v. 2, p. 1-34.
946 Krause, A.J., Mills, B.J., Zhang, S., Planavsky, N.J., Lenton, T.M., and Poulton, S.W., 2018,
947 Stepwise oxygenation of the Paleozoic atmosphere: Nature Communications, v. 9, p. 1–10.
948 Jorgensen, B.B., 1982, Mineralisation of organic matter in the sea bed—the role of sulphate
949 reduction: Nature, v. 296, p. 643–645.
950 Lee, J.H., Chen, J., and Chough, S.K., 2015, The middle–late Cambrian reef transition and related
951 geological events: a review and new view: Earth-Sci. Rev., v. 145, p. 66–84.
952 Li, D.D., Zhang, X.L., Hu, D.P., Chen, X.Y., Huang, W., Zhang, X., Li, M.H., Qin, L.P., Peng,
953 S.C., and Shen, Y.A, 2018, Evidence of a large $\delta^{13}C_{carb}$ and $\delta^{13}C_{org}$ depth gradient for
954 deep-water anoxia during the late Cambrian SPICE event: Geology, v. 46, p. 631–634.
955 Lochman-Balk, C., 1970, Upper Cambrian faunal patterns on the craton: Geol. Soc. Am. Bull., v.
956 81, p. 3197-3224.
957 Longacre, S.A., 1970, Trilobites of the Upper Cambrian Ptychaspid Biomere Wilberns Formation,
958 Central Texas: Paleontol. Soc. Mem., v. 44, p. 1–68.
959 Lu, Y.H., and Lin, H.L., 1989, The Cambrian trilobites of western Zhejiang: Palaeontologia
960 Sinica, v. 178(25), 287 pp.
961 Marenco, P.J., Corsetti, F.A., Kaufman, A.J., and Bottjer, D.J., 2008, Environmental and
962 diagenetic variations in carbonate associated sulfate: an investigation of CAS in the lower
963 Triassic of the western USA: Geochim. Cosmochim. Acta, v. 72, p. 1570–1582.
964 Marshall, C.R., 2006, Explaining the Cambrian "explosion" of animals: Ann. Rev. Earth Planet.
965 Sci., v. 34, p. 355–384.
966 Marshall, J.D., 1992, Climatic and oceanographic isotopic signals from the carbonate rock record
967 and their preservation: Geological Magazine, v. 129, p. 143–160.
968 Matthews, R.K., and Al-Husseini, M.I., 2010, Orbital-forcing glacio-eustasy: A
969 sequence-stratigraphic time scale: GeoArabia, v. 15, p. 155–167.
970 Mazumdar, A., Peketi, A., Joao, H., Dewangan, P., Borole, D.V., and Kocherla, M., 2012,
971 Sulfidization in a shallow coastal depositional setting: Diagenetic and palaeoclimatic
972 implications: Chemical Geology, v. 322-323, p. 68–78.
973 McLennan, S.M., 2001. Relationships between the trace element composition of sedimentary
974 rocks and upper continental crust: Geochem. Geophys. Geosyst. 2 (2000GC000109, 24 pp.).

975 Moysiuk, J., and Caron, J.B., 2019, Burgess Shale fossils shed light on the agnostid problem:
976 Proceedings of the Royal Society B, v. 286(1894), p. 20182314.
977 Öpik, A.A., 1966, The Early Upper Cambrian crisis and its correlation: J. Proc. Roy. Soc. New
978 South Wales, v. 100, p. 9–14.
979 Palmer, A.R., 1965a, Biomere: A new kind of biostratigraphic unit: J. Paleontol., v. 39, p. 149–
980 153.
981 Palmer, A.R., 1965b, Trilobites of the Late Cambrian Pterocephaliid Biomere in the Great Basin,
982 United States: Geol. Surv. Prof. Pap., v. 493, 153 pp.
983 Palmer, A.R., 1979, Biomere boundaries re-examined: Alcheringa, v. 3, p. 33–41.
984 Palmer, A.R., 1984, The biomere problem — evolution of an idea: J. Paleontol., v. 58, p. 599–611.
985 Peng, S.C., 2005, Potential candidate stratotypes for the levels of *Lejopyge laevigata* and
986 *Agnostotes orientalis*: Acta Micropaleontologica Sinica, v. 22, p. 148–149.
987 Peng, S.C., and Robison, R.A., 2000, Agnostoid biostratigraphy across the Middle-Upper
988 Cambrian boundary in China: Paleontological Society Memoir 53, Journal of Paleontology,
989 v. 74, Supplement p. 1–104.
990 Peng, S.C., Babcock, L.E., and Lin, H.L., 2004, Polymerid trilobites from the Cambrian of
991 northwestern Hunan, China, volume 1: Corynexochida, Lichida, and Asaphida, Beijing,
992 Science Press, 333 pp.
993 Peng, S.C., Babcock, L. E., and Lin, H.L., 2005, Polymerid trilobites from the Cambrian of
994 northwestern Hunan, China, volume 2: Ptychopariida, Eodiscida, and Undetermined forms,
995 Beijing, Science Press, 355 pp.
996 Peng, S.C., Babcock, L., Robison, R., Lin, H.L., Rees, M., and Saltzman, M., 2004, Global
997 standard stratotype-section and point (GSSP) of the Furongian Series and Paibian Stage
998 (Cambrian): Lethaia, v. 37, p. 365–379.
999 Peng, S.C., Babcock, L.E., Zuo, J.X, Lin, H.L., Zhu, X.J., Yang, X.F., Robison, R.A., Qi, Y.P., and
1000 Bagnoli, G., 2006, Proposed GSSP for the base of Cambrian Stage 7, coinciding with the first
1001 appearance of *Lejopyge laevigata*, Hunan, China: Palaeoworld, v. 15, p. 367–383.
1002 Peng, S.C., Babcock, L.E., Zuo, J.X., Lin, H.L., and Chen, Y.A., 2009, The Global Boundary
1003 Stratotype Section and Point (GSSP) of the Guzhangian Stage (Cambrian) in the Wuling
1004 Mountains, Northwestern Hunan, China: Episodes, v. 32, p. 41–55.
1005 Peng, S.C., Babcock, L.E., and Cooper, R.A., 2012, The Cambrian Period, pp. 437-488. In:
1006 Gradstein, F.M., Ogg, J.G., Schmitz, M.D., Ogg, G.M. (eds.), The Geologic Time Scale 2012:
1007 Elsevier, New York.
1008 Perfetta, P.J., Shelton, K.L., and Stitt, J.H., 1999, Carbon isotope evidence for deep-water invasion
1009 at the Marjumiid-Pterocephaliid biomere boundary, Black Hills, USA: A common origin for
1010 biotic crises on Late Cambrian shelves: Geology, v. 27, p. 403–406.
1011 Pratt, B.R., 1992, Trilobites of the Marjuman and Steptoean stages (Upper Cambrian),
1012 Rabbitkettle Formation, southern Mackenzie Mountains, northwest Canada: Palaeontogr.
1013 Canad., v. 9, 179 pp.

1014 Present, T.M., Gutierrez, M., Paris, G., Kerans, C., Grotzinger, J.P., and Adkins, J.F., 2019,
1015 Diagenetic controls on the isotopic composition of carbonate–associated sulphate in the
1016 Permian Capitan Reef Complex, West Texas: Sedimentology, v. 66, p. 2605–2626.
1017 Pulsipher, M.A., Schiffbauer, J.D., Jeffrey, M.J., Huntley, J.W., Fike, D.A., and Shelton, K.L.,
1018 2021, A meta-analysis of the Steptoean positive carbon isotope excursion: The SPICEraq
1019 database: Earth-Science Reviews, v. 212, p. 103442.
1020 Rasmussen, C.M.Ø., and Harper, D.A.T., 2011, Interrogation of distributional data for the End
1021 Ordovician crisis interval: Where did disaster strike?: Geological Journal, v. 46, p. 478–500.
1022 Rasmussen, C.M.Ø., Kröger, B., Nielsen, M.L., Colmenar, J., 2019, Cascading trend of Early
1023 Paleozoic marine radiations paused by Late Ordovician extinctions: Proc. Natl. Acad. Sci.
1024 USA, v. 116, p. 7207–7213.
1025 Richardson, J.A., Lepland, A., Hints, O., Prave, A. R., Gilhooly III, W.P., Bradley, A.S., and Fike,
1026 D.A., 2021, Effects of early marine diagenesis and site-specific depositional controls on
1027 carbonate-associated sulfate: Insights from paired S and O isotopic analyses: Chemical
1028 Geology, v. 584, p. 120525.
1029 Richardson, J.A., Newville, M., Lanzirotti, A., Webb, S.M., Rose, C.V., Catalano, J.G., and Fike,
1030 D. A., 2019, Depositional and diagenetic constraints on the abundance and spatial variability
1031 of carbonate-associated sulfate: Chemical Geology, v. 523, p. 59-72.
1032 Rieboldt, S.E., 2005, Inarticulate Brachiopods of the late Maijumiid and Pterocephaliid Biomeres
1033 (late Middle- early Late Cambrian) of West-Central Utah and East-Central Nevada, U.S.A.
1034 [Ph.D. thesis]: Berkeley, University of California, 311 pp.
1035 Rowell, A.J., and Brady, M.J., 1976, Brachiopods and biomeres: Brigham Young Univ. Geol.
1036 Studies, v. 23, p. 165–180.
1037 Runkel, A.C., McKay, R.M., and Palmer, A.R., 1998, Origin of a classic cratonic sheet sandstone:
1038 Stratigraphy across the Sauk II–Sauk III boundary in the Upper Mississippi Valley:
1039 Geological Society of America Bulletin, v. 110, p. 188–210.
1040 Rushton, A. W. A., and Hughes, N. C., 1996, Biometry, systematics and biogeography of the late
1041 Cambrian trilobite *Maladioidella abdita*: Transactions of the Royal Society of Edinburgh:
1042 Earth Sciences, v. 86, p. 247–256.
1043 Saltzman, M.R., 2005, Phosphorus, nitrogen, and the redox evolution of the Paleozoic oceans:
1044 Geology, v. 33, p. 573–576.
1045 Saltzman, M.R., and Thomas, E., 2012, Carbon isotope stratigraphy, pp. 207-232. In: Gradstein,
1046 F.M., Ogg, J.G., Schmitz, M.D., Ogg, G.M., eds., The Geologic Time Scale 2012: Elsevier,
1047 New York.
1048 Saltzman, M.R., Runnegar, B., and Lohmann, K.C., 1998, Carbon isotope stratigraphy of Upper
1049 Cambrian (Steptoean Stage) sequences of the eastern Great Basin: Record of a global
1050 oceanographic event: Geol. Soc. Am. Bull., v. 110, p. 285–297.
1051 Saltzman, M.R., Ripperdan, R.L., Brasier, M.D., Lohmann, K.C., Robison, R.A., Chang, W.T.,
1052 Peng, S., Ergaliev, E.K., and Runnegar, B., 2000, A global carbon isotope excursion (SPICE)

during the Late Cambrian: relation to trilobite extinctions, organic-matter burial and sea level: Palaeogeogr. Palaeoclimatol. Palaeoecol., v. 162, p. 211–223.

Saltzman, M.R., Cowan, C.A., Runkel, A.C., Runnegar, B., Stewart, M.C., and Palmer, A.R., 2004, The Late Cambrian SPICE ($\delta^{13}C$) event and the Sauk II–Sauk III regression: new evidence from Laurentian Basins in Utah, Iowa, and Newfoundland: J. Sed. Res., v. 74, p. 365–377.

Saltzman, M.R., Young, S.A., Kump, L. R., Gill, B.C., Lyons, T.W., Runnegar, B., and Berner, R.A., 2011, Pulse of atmospheric oxygen during the Late Cambrian: Proc. Natl. Acad. Sci. USA, v. 108, p. 3876–3881.

Schiffbauer, J.D., Huntley, J.W., Fike, D.A., Jeffrey, M.J., Gregg, J.M., and Shelton, K.L., 2017, Decoupling biogeochemical records, extinction, and environmental change during the Cambrian SPICE event: Sci. Adv., v. 3, e1602158.

Schrag, D.P., Higgins, J.A., Macdonald, F.A., and Johnston, D.T., 2013, Authigenic carbonate and the history of the global carbon cycle: Science, v. 339, p. 540-543.

Scott, C., Lyons, T.W., 2012. Contrasting molybdenum cycling and isotopic properties in euxinic versus non-euxinic sediments and sedimentary rocks: Refining the paleoproxies: Chem. Geol., v. 324, p. 19-27.

Servais, T., Lehnert, O., Li, J., Mullins, G.L., Munnecke, A., Nuetzel, A., and Vecoli, M., 2008, The Ordovician Biodiversification: revolution in the oceanic trophic chain: Lethaia, v. 41, p. 99–109.

Servais, T., Owen, A.W., Harper, D.A., Kröger, B., and Munnecke, A., 2010, The Great Ordovician Biodiversification Event (GOBE): the palaeoecological dimension: Palaeogeogr. Palaeoclimatol. Palaeoecol., v. 294, p. 99–119.

Sørensen, A.L., Nielsen, A.T., Thibault, N., Zhao, Z., Schovsbo, N.H., and Dahl, T.W., 2020, Astronomically forced climate change in the late Cambrian: Earth and Planetary Science Letters, v. 548, 116475.

Stitt, J.H., 1971, Repeating evolutionary pattern in Late Cambrian trilobite biomeres: J. Paleontol., v. 45, p. 178–181.

Stitt, J.H., 1975, Adaptive radiation, trilobite paleoecology and extinction, Ptychaspidid Biomere, Late Cambrian of Oklahoma: Fossils and Strata, v. 4, p. 381–390.

Stitt, J. H., Rucker, J. D., Boyer, N. D., and Hart, W. D., 1994, New *Elvinia* Zone (Upper Cambrian) trilobites from new localities in the Collier Shale, Ouachita Mountains, Arkansas: Journal of Paleontology, v. 68, p. 518–523.

Stouffer, R.J., Yin, J., Gregory, J.M., Dixon, K.W., Spelman, M.J., Hurlin, W., Weaver, A.J., Eby, M., Flato, G.M., Hasumi, H., Hu, A., Jungclaus, J.H., Kamenkovich, I.V., Levermann, A., Montoya, M., Murakami, S., Nawrath, S., Oka, A., Peltier, W.R., Robitaille, D.Y., Sokolov, A., Vettoretti, G., and Weber, S.L., 2006, Investigating the causes of the response of the thermohaline circulation to past and future climate changes: J. Clim., v. 19, p. 1365–1387.

Swart, P.K., 2008, Global synchronous changes in the carbon isotopic composition of carbonate sediments unrelated to changes in the global carbon cycle: Proceedings of the National

1092 Academy of Sciences, v. 105, p. 13741–13745.
1093 Swart, P.K., 2015, The geochemistry of carbonate diagenesis: The past, present and future:
1094 Sedimentology, v. 62, p. 1233–1304.
1095 Swart, P.K., and Kennedy, M.J., 2012, Does the global stratigraphic reproducibility of $\delta^{13}C$ in
1096 Neoproterozoic carbonates require a marine origin? A Pliocene–Pleistocene comparison:
1097 Geology, v. 40, p. 87–90.
1098 Taylor, J.F., 2006, History and status of the biomere concept: Assoc. Australas. Paleontol. Mem.
1099 32, p. 247–265.
1100 Thickpenny, A., 1987, Palaeo-oceanography and depositional environment of the Scandinavian
1101 Alum Shales: sedimentological and geochemical evidence: Marine clastic sedimentology.
1102 Springer, Dordrecht, p. 156–171.
1103 Trotter, J.A., Williams, I.S., Barnes, C.R., Lecuyer, C., and Nicoll, R.S.., 2008, Did cooling oceans
1104 trigger Ordovician biodiversification? evidence from conodont thermometry: Science, v. 321,
1105 p. 550–554.
1106 Westrop, S.R., 1988, Trilobite diversity patterns in an Upper Cambrian stage: Paleobiology, v. 14,
1107 p. 401–409.
1108 Westrop, S.R., and Cuggy, M.B., 1999, Comparative paleoecology of Cambrian trilobite
1109 extinctions: J. Paleontol., v. 73, p. 337–354.
1110 Westrop, S.R., and Ludvigsen, R., 1987, Biogeographic control of trilobite mass extinction at an
1111 Upper Cambrian "biomere" boundary: Paleobiology, v. 13, p. 84–99.
1112 Whitney, F.A., Crawford, W.R., and Harrison, P.J., 2005, Physical processes that enhance nutrient
1113 transport and primary productivity in the coastal and open ocean of the subarctic NE Pacific.
1114 Deep-Sea Res. II, v. 52, p. 681–706.
1115 Wotte, T., Shields-Zhou, G.A., and Strauss, H., 2012, Carbonate-associated sulfate: Experimental
1116 comparisons of common extraction methods and recommendations toward a standard
1117 analytical protocol: Chemical Geology, v. 326, p. 132–144.
1118 Wotte, T., Skovsted, C.B., Whitehouse, M.J., and Kouchinsky, A., 2019, Isotopic evidence for
1119 temperate oceans during the Cambrian explosion: Scientific Reports, v. 9, 6330, 9 pp.
1120 Wunsch, C., 2002, What is the thermohaline circulation?: Science, v. 298, p. 1179-1181.
1121 Zeebe R.E., and Wolf-Gladrow D.A., 2001, CO_2 in Seawater: Equilibrium, Kinetics, Isotopes:
1122 Elsevier Oceanography Series, 346 pp.
1123 Zhan, R.B., Liu, J.B., Percival, I.G., Jin, J.S., and Guipeng, LI.., 2010, Biodiversification of Late
1124 Ordovician *Hirnantia* fauna on the Upper Yangtze Platform, South China: Science China D:
1125 Earth Sciences, v. 53, p. 1800–1810.
1126 Zhao, M.Y., Zheng, Y.F., and Zhao, Y.Y., 2016, Seeking a geochemical identifier for authigenic
1127 carbonate: Nature communications, v. 7, p. 1-7.
1128 Zhang, L., Algeo, T.J., Zhao, L.S., Chen, Z.Q., Zhao, H., Zhang, Z.H., and Li, C., 2022, Linkage
1129 of the late Cambrian microbe-metazoan transition (MMT) to shallow-marine oxygenation
1130 during the SPICE event. Global and Planetary Change, v. 213, p. 103798.
1131 Zhang, S.H., Fan, J.X., Morgan, C.A., Henderson, C.M., and Shen, S.Z., 2021, Quantifying the

middle–late Cambrian trilobite diversity pattern in South China: Palaeogeography, Palaeoclimatology, Palaeoecology, v. 570, p. 110361.

Zhang, Y.G., Yang, T., Hohl, S.V., Zhu, B., He, T.C., Pan, W.Q., Chen, Y.Q., Yao, X.Z., and Jiang, S.Y., 2020, Seawater carbon and strontium isotope variations through the late Ediacaran to late Cambrian in the Tarim Basin: Precambr. Res., v. 345, p. 105769.

Zhou, L., Algeo, T.J., Shen, J., Hu, Z.F., Gong, H.M., Xie, S.C., Huang, J.H., and Gao, S., 2015, Changes in marine productivity and redox conditions during the Late Ordovician Hirnantian glaciation: Palaeogeography, Palaeoclimatology, Palaeoecology, v. 420, p. 223–234.

Zhou, Z.Y., and Zhen, Y.Y., 2008, Trilobite Record of China: Beijing, Science Press, 401 pp.

Zhu, M.Y., Yang, A.H., Yuan, J.L., Li, G.X., Zhang, J.M., Zhao, F.C., Ahn, S., and Miao, L.Y, 2018, Cambrian integrative stratigraphy and timescale of China: Sci. China D: Earth Sci., v. 62, p. 25–60.

Zuo, J., Peng, S., Qi, Y., Zhu, X., Bagnoli, G., and Fang, H., 2018, Carbon-isotope excursions recorded in the Cambrian system, South China: Implications for mass extinctions and sea-level fluctuations: Journal of Earth Science, v. 29, p. 479–491.

Żylińska, A., 2001, Late Cambrian trilobites from the Holy Cross Mountains, central Poland: Acta Geologica Polonica, v. 51, p. 333–383.

Żylińska, A., 2002, Stratigraphic and biogeographic significance of Late Cambrian trilobites from Łysogóry (Holy Cross Mountains, central Poland): Acta Geologica Polonica, v. 52, p. 217–238.

Figure captions:

Fig. 1. Paleogeographic maps of the Late Cambrian world (A), South China Craton (B), and local maps of Guzhang County (C) and Jiangshan urban area (D), showing locations of Wangcun, Duibian A and B, and other globally distributed SPICE sections discussed in the text. Map A is from https://deeptimemaps.com authorized by Colorado Plateau Geosystems Inc. Map B is adapted from Li et al. (2018).

Fig. 2. Trilobite and isotopic data for the Wangcun section: (A) trilobite species ranges, (B) trilobite species diversity; (C) carbonate (carb) $\delta^{13}C$ (‰ VPDB); and (D) carbonate-associated sulfate (CAS) $\delta^{34}S$ (‰ CDT). In panel A, trilobite range data are from Peng et al. (2009), with red and blue lines representing actual range and range-through data, respectively. The base of the Paibian and the base of the Jiangshanian have been correlated from Duibian A based on trilobite-carbon isotope biochemostratigraphy from Zuo et al. (2018). The gray fields represent the stratigraphic extent of SPICE; 'Early SPICE' is newly defined herein, and its base implies an earlier onset of the SPICE than inferred in some earlier studies (see Section 2.5). Abbreviations: *A. inexpectans* = *Agnostus inexpectans*; *Ag. orientalis* = *Agnostotes orientalis*; *C. plumula* = *Corynexochus plumula*; *E. rectang.* = *Erixanium rectangularis*; *G. reticulatus* = *Glyptagnostus*

reticulatus; *G.s.* = *Glyptagnostus stolidotus*; *Go.n.* = *Goniagnostus nathorsti*; *L.a.* = *Lejopyge armata*; *Li.r.* = *Linguagnostus reconditus*; *L.l.* = *Lejopyge laevigata*; *P.a.* = *Ptychagnostus aculeatus*; *P.p.* = *Ptychagnostus punctuosus*; *Pr.b.* = *Proagnostus bulbus*; *E.* = *Erixanium*; *Ir.* = *Irvingella*; *T.* = *Tomagnostella*; Jiangshan. = Jiangshanian; Wu. = Wuliuan.

Fig. 3. Trilobite and isotopic data for the Duibian A section: (A) trilobite species ranges, (B) trilobite species diversity; (C) carbonate (carb) $\delta^{13}C$ (‰ VPDB); and (D) carbonate-associated sulfate (CAS) $\delta^{34}S$ (‰ CDT). Trilobite data from Peng et al. (2012). See Figure 2 caption for other details.

Fig. 4. Trilobite and isotopic data for the Duibian B section: (A) trilobite species ranges, (B) trilobite species diversity; (C) carbonate (carb) $\delta^{13}C$ (‰ VPDB); and (D) carbonate-associated sulfate (CAS) $\delta^{34}S$ (‰ CDT). Trilobite data from Peng et al. (2012). See Figure 2 caption for other details.

Fig. 5. Trilobite and elemental data for the Wangcun section: (A) trilobite species diversity; (B) total organic carbon (TOC); (C) Al_2O_3; (D) U_{EF}; (E) Mo_{EF}; and (F) C_{org}/P. Red circles represent samples with low detrital content (Al_2O_3 < 1%) that may result in artificially high U_{EF} and Mo_{EF} values. For abbreviations refer to Figure 2.

Fig. 6. Trilobite and elemental data for the Duibian A section: (A) trilobite species diversity; (B) total organic carbon (TOC); (C) Al_2O_3; (D) U_{EF}; (E) Mo_{EF}; and (F) C_{org}/P. For other details see Figure 5 caption; for abbreviations refer to Figure 2.

Fig. 7. Trilobite and elemental data for the Duibian B section: (A) trilobite species diversity; (B) total organic carbon (TOC); (C) Al_2O_3; (D) U_{EF}; (E) Mo_{EF}; and (F) C_{org}/P. For other details see Figure 5 caption; for abbreviations refer to Figure 2.

Fig. 8. Seawater redox conditions in Wangcun, Duibian A and B sections, based on (A-C) Mo_{EF} vs. U_{EF} and (D) TOC vs. P. Panels A-C are after Algeo and Tribovillard (2009): U_{EF} values are mostly 3-10 in suboxic, and Mo_{EF} values > 10 in anoxic environments. Redox thresholds in panel D are after Algeo and Ingall (2007): C_{org}:P ratios are mostly < 50 in oxic, 50 to 100-125 in suboxic and > 100-125 in anoxic environments. In panel D, all data are shown without reference to Al_2O_3 content, because the C_{org}:P proxy is independent of Al_2O_3 content.

Fig. 9. Global comparisons of (A) $\delta^{13}C_{carb}$ (‰ VPDB), (B) $\delta^{34}S_{CAS}$ (‰ CDT), (C) $\delta^{34}S_{pyrite}$ (‰ CDT), and (D) $\Delta^{34}S_{(CAS\text{-}py)}$ profiles. Data sources: Shingle Pass (Saltzman et al., 1998; Gill et al., 2007); Lawson Cove and TE-1 Texas County Core (Gill et al., 2011); Mount Whelan Core (Saltzman et al., 2000; Gill et al., 2011); Wangcun, Duibian A and B (this study). All profiles were replotted and smoothed using the Drumian-Guzhangian (~500.5 Ma), Guzhangian-Paibian (~497 Ma), and Paibian-Jiangshanian (~494 Ma) boundaries as age tie-points, and assuming isochroneity of the SPICE peak globally. For sections containing incomplete Guzhangian or Jiangshanian stages, age assignments were made assuming a constant sedimentation rate based on the Paibian stage. Notes: (1) peak $\delta^{34}S_{CAS}$ values occurred during the Rising SPICE (Gill et al., 2011; this

study); (2) for Shingle Pass, maximum $\delta^{13}C_{carb}$ is reached slightly below a facies change, so the peak SPICE interval may have been truncated (Saltzman et al., 2000; Gill et al., 2011). Color scheme: green = surface layer, blue = intermediate water depth, and black = deep layer. Note existence of a depth-related gradient for each isotopic system. See the Supplemental file for descriptions of the sedimentary settings of the sections analyzed here.

Fig. 10. Summary figure for regional and global marine proxies during the SPICE event: (A) $\delta^{13}C_{carb}$ (‰ VPDB), (B) $\delta^{34}S_{CAS}$ (‰ CDT), (C) seawater redox, and (D) trilobite diversity of South China (this study); (E) trilobite diversity of Laurentia, based on House Range (Utah), Highland Range (Nevada), Desert Range (Nevada) and Royer Ranch (Oklahoma) sections (Palmer, 1978, 1984); (F) sea-level changes of Laurentia, based on studies in Upper Mississippi Valley (Runkel et al., 1998); (G) seawater redox conditions of Baltica, based on studies of Mo-U enrichments and Fe speciation in Andrarum-3 drillcore (Gill et al., 2011); (H) global seawater redox conditions, based on studies of carbonate U-isotopes in Whelan no. 1 drillcore, Australia (Dahl et al., 2014); and (I) general global SSTs, based on studies of Saltzman (2005), Matthews and Al-Husseini (2010) and Al-Husseini (2017). In panels D and E, colors refer to Pre- and Early SPICE vs. Rising and Falling SPICE vs. Post-SPICE. In panel E, blue horizontal lines are counted diversity from Palmer (1984). In panels D and E, due to lack of biostratigraphic constraints (Palmer, 1984), correlations of trilobite diversity curves are based on diversity peaks. For abbreviations see Figures 2-4.

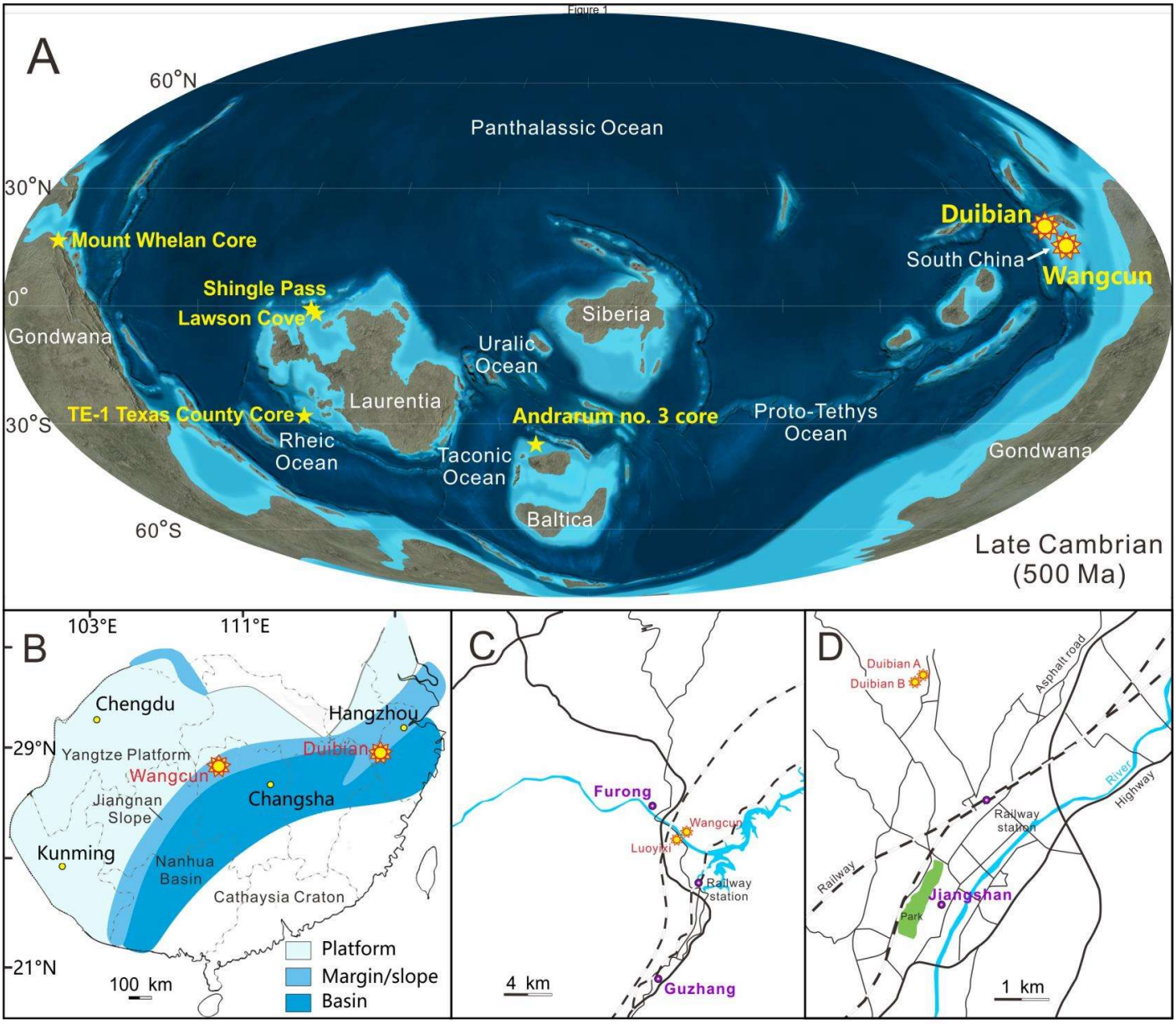
Figure 1
A
60°N
30°N
0°
30°S
60°S
Panthalassic Ocean
Mount Whelan Core
Shingle Pass
Lawson Cove
Gondwana
TE-1 Texas County Core
Rheic Ocean
Laurentia
Uralic Ocean
Siberia
Andrarum no. 3 core
Taconic Ocean
Baltica
Proto-Tethys Ocean
Gondwana
Duibian
South China
Wangcun
Late Cambrian (500 Ma)
B
103°E
111°E
29°N
21°N
Chengdu
Hangzhou
Yangtze Platform
Duibian
Wangcun
Changsha
Jiangnan Slope
Kunming
Nanhua Basin
Cathaysia Craton
100 km
Platform
Margin/slope
Basin
C
Furong
Wangcun
Luoyixi
Railway station
4 km
Guzhang
D
Duibian A
Duibian B
Asphalt road
River
Highway
Railway station
Railway
Jiangshan
Park
1 km

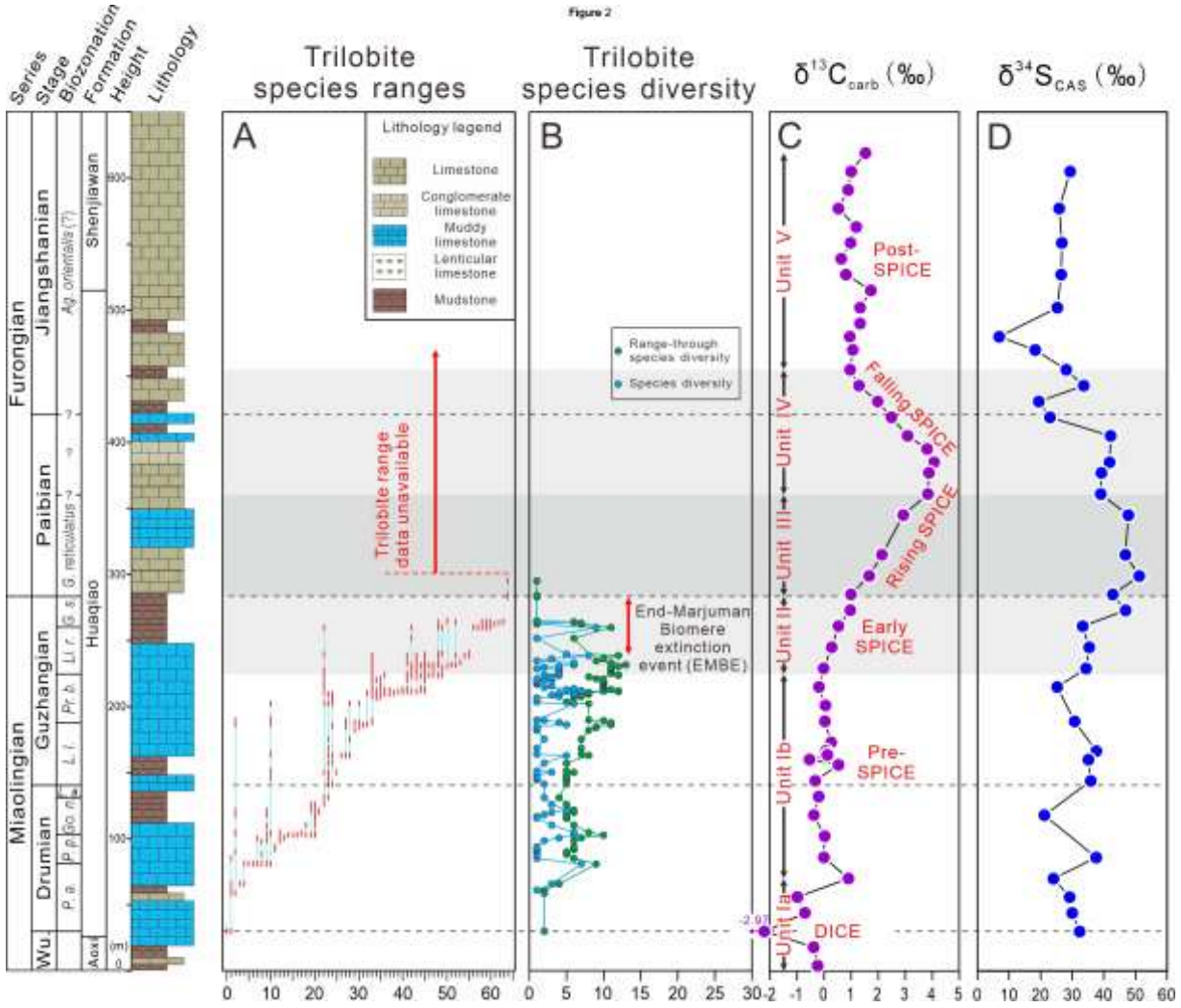
Figure 2
Series
Stage
Biozonation
Formation
Height
Lithology
Furongian
Miaolingian
Jiangshanian
Paibian
Guzhangian
Drumian
Wu.
Ag. orientalis (?)
G. reticulatus
Shenjiawan
Huaqiao
Aox.
Trilobite species ranges
Trilobite species diversity
δ13Ccarb (‰)
δ34SCAS (‰)
A
B
C
D
Lithology legend
Limestone
Conglomerate limestone
Muddy limestone
Lenticular limestone
Mudstone
Trilobite range data unavailable
Range-through species diversity
Species diversity
End-Marjuman Biomere extinction event (EMBE)
Unit V
Unit IV
Unit III
Unit II
Unit Ib
Unit Ia
Post-SPICE
Falling SPICE
Rising SPICE
Early SPICE
Pre-SPICE
DICE
-2.97
0 10 20 30 40 50 60
0 5 10 15 20 25 30
-2 -1 0 1 2 3 4 5
0 10 20 30 40 50 60

Figure 3

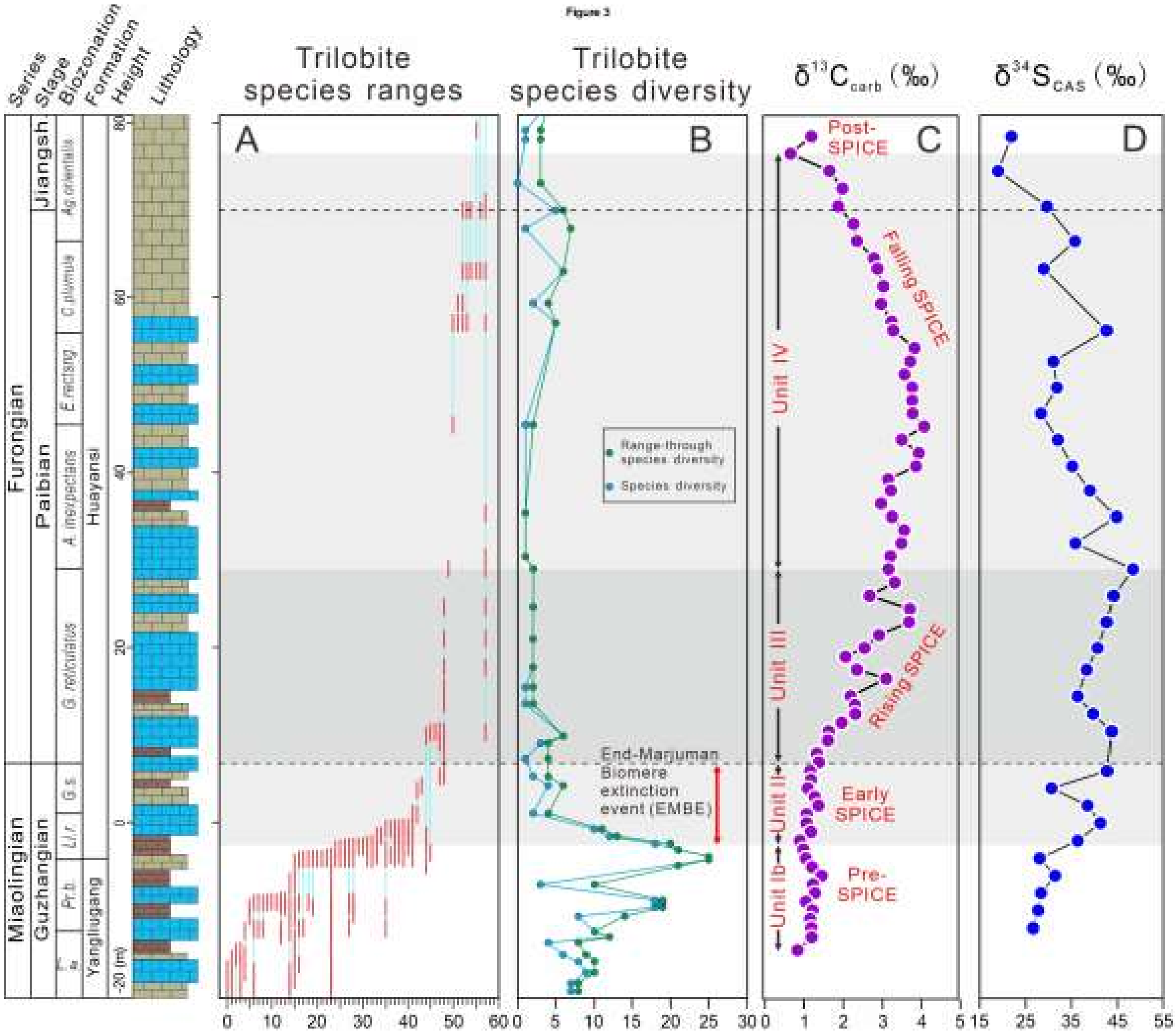

Series
Stage
Biozonation
Formation
Height
Lithology
Furongian
Miaolingian
Paibian
Guzhangian
Jiangsh.
Huayansi
Yangliugang
Ag. orientalis
C. plumula
E. rectang.
A. inexpectans
G. reticulatus
G.s.
Li.r.
Pr.b.
Trilobite species ranges
Trilobite species diversity
$\delta^{13}C_{carb}$ (‰)
$\delta^{34}S_{CAS}$ (‰)
A
B
C
D
Range-through species diversity
Species diversity
End-Marjuman Biomere extinction event (EMBE)
Post-SPICE
Falling SPICE
Rising SPICE
Early SPICE
Pre-SPICE
Unit IV
Unit III
Unit II
Unit Ib

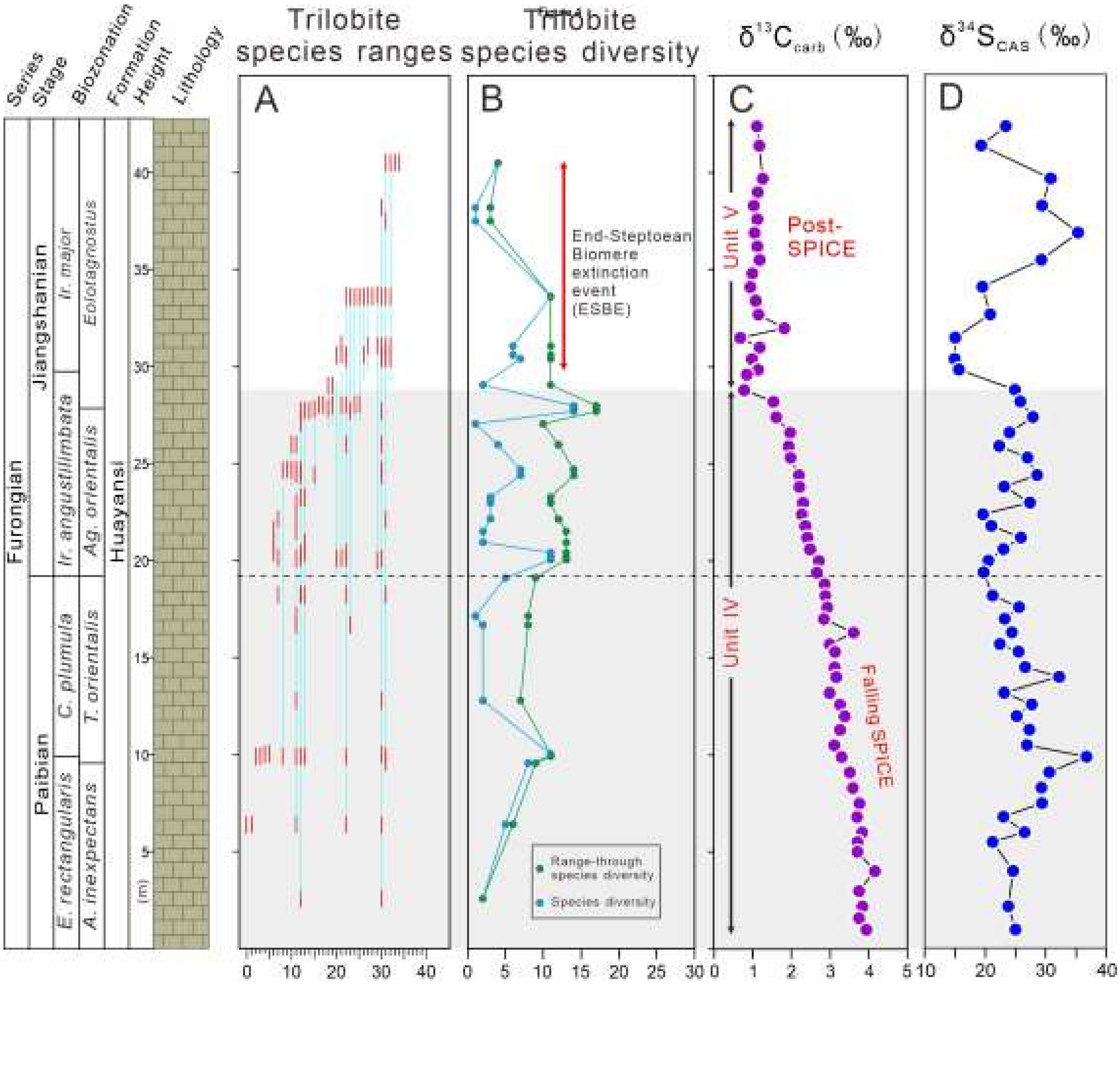

Series
Stage
Biozonation
Formation
Height
Lithology
Furongian
Paibian
Jiangshanian
E. rectangularis
C. plumula
Ir. angustilimbata
Ir. major
A. inexpectans
T. orientalis
Ag. orientalis
Eolotagnostus
Huayansi
Trilobite species ranges
Trilobite species diversity
$\delta^{13}C_{carb}$ (‰)
$\delta^{34}S_{CAS}$ (‰)
A
B
C
D
End-Steptoean Biomere extinction event (ESBE)
Range-through species diversity
Species diversity
Post-SPICE
Falling SPICE
Unit V
Unit IV

Figure 5

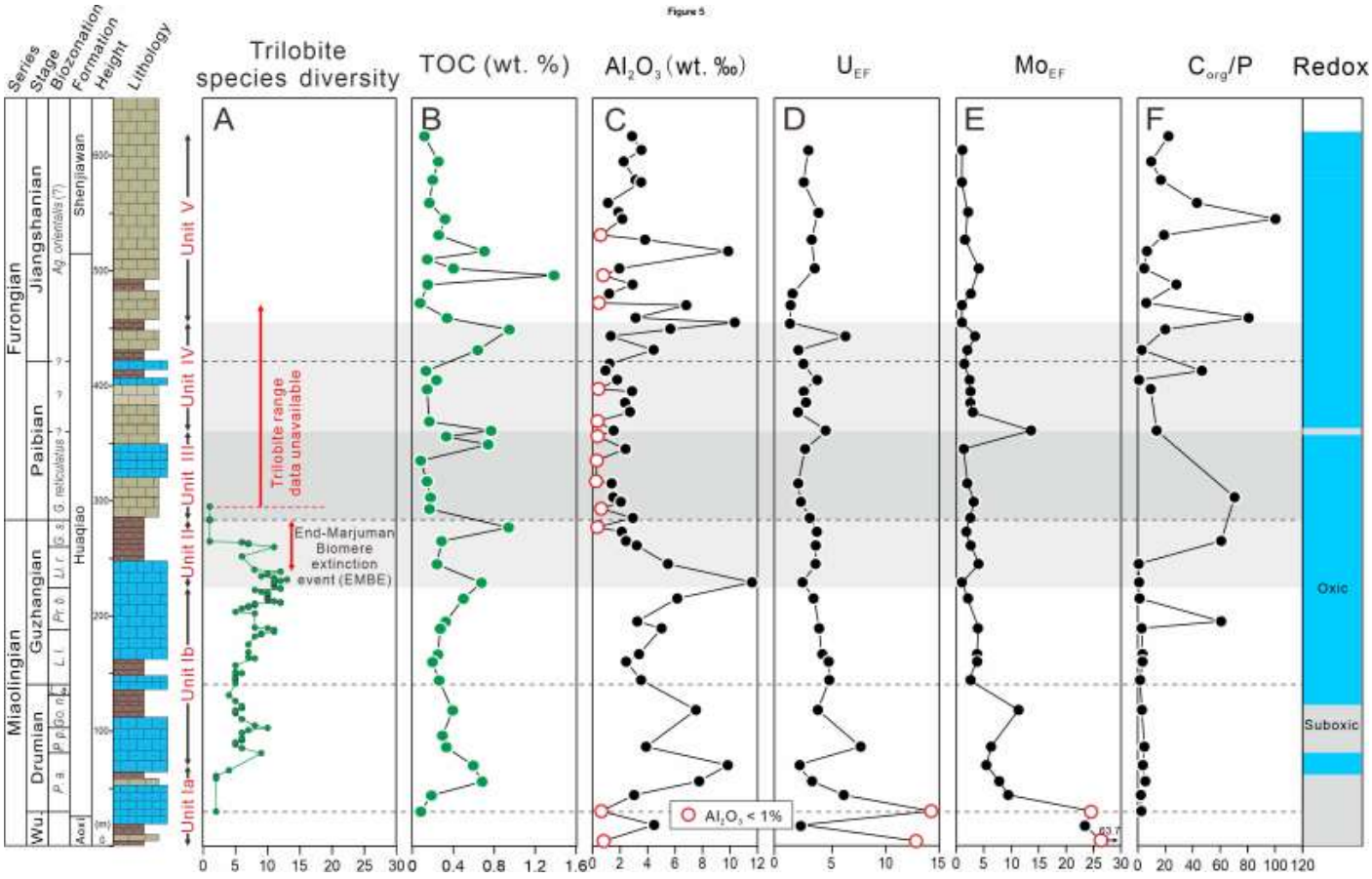

Figure 6

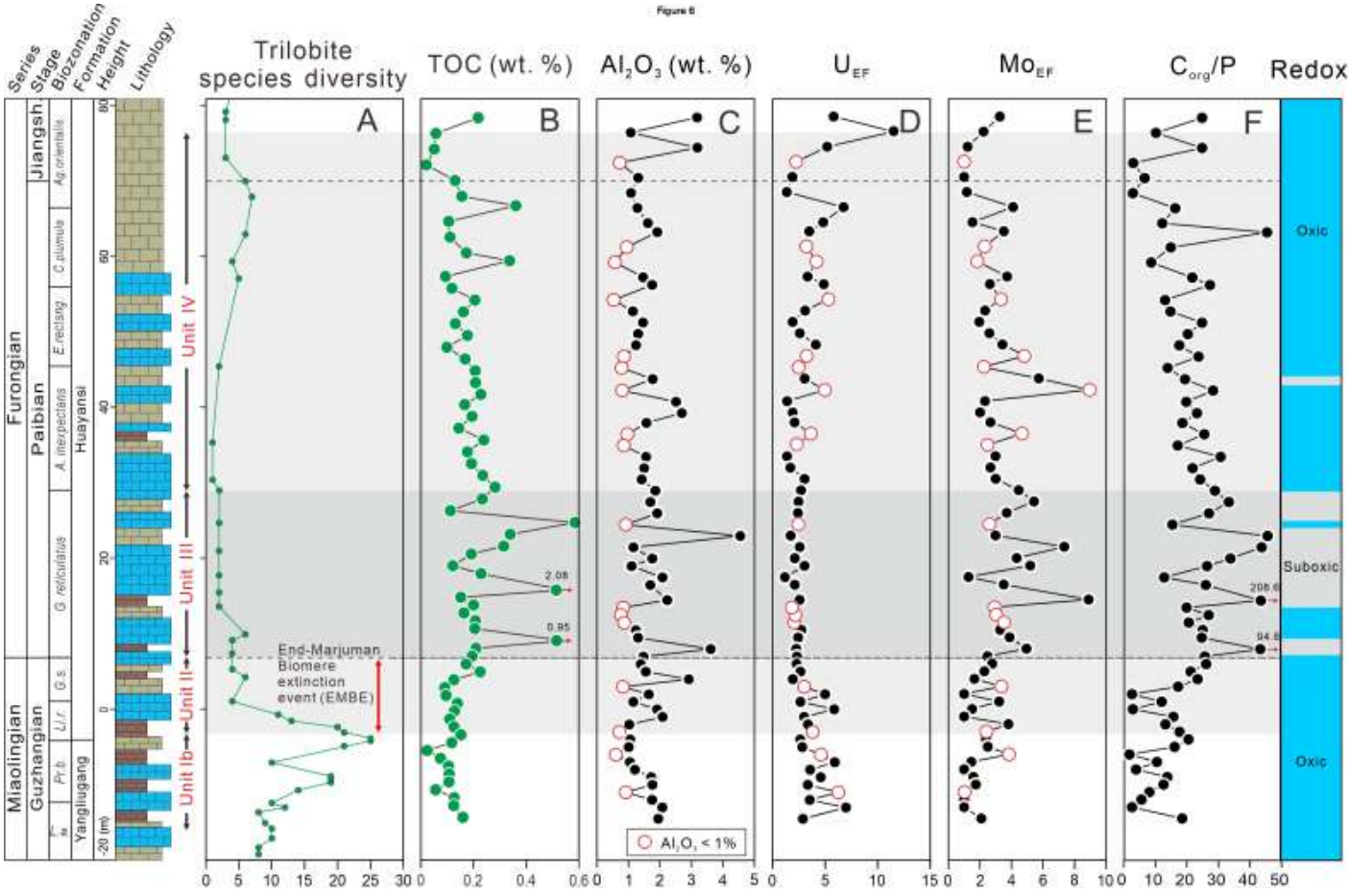

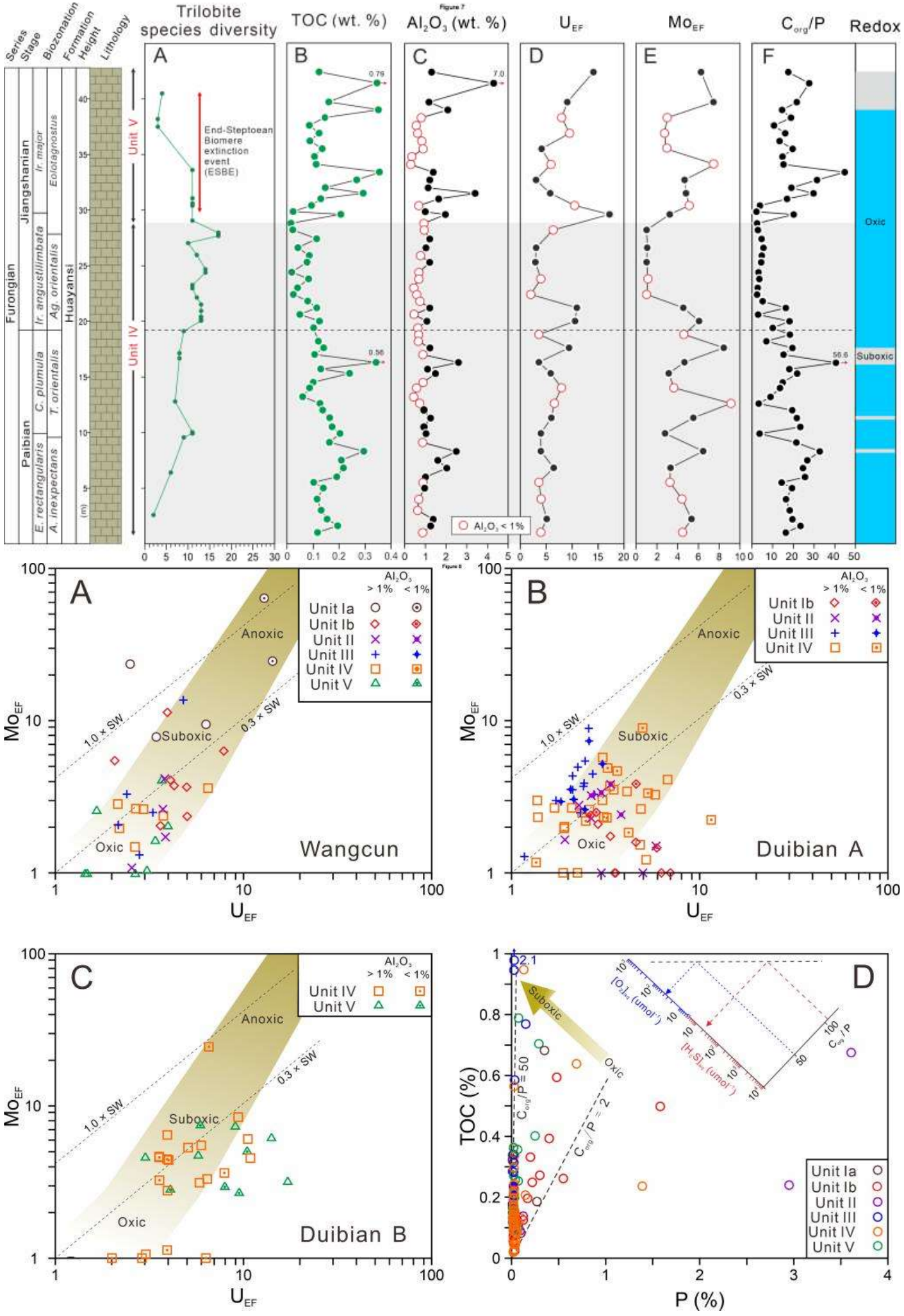
Series
Stage
Biozonation
Formation
Height
Lithology
Furongian
Jiangshanian
Paibian
Ir. major
Ir. angustilimbata
C. plumula
E. rectangularis
A. inexpectans
Eolotagnostus
Ag. orientalis
T. orientalis
Huayansi
(m)
Unit V
Unit IV
Trilobite species diversity
End-Steptoean Biomere extinction event (ESBE)
TOC (wt. %)
0.79
0.56
Al_2O_3 (wt. %)
7.0
Al_2O_3 < 1%
U_{EF}
Mo_{EF}
C_{org}/P
56.6
Redox
Oxic
Suboxic
A
B
C
D
E
F
Anoxic
Suboxic
Oxic
1.0 × SW
0.3 × SW
Al_2O_3
> 1%
< 1%
Unit Ia
Unit Ib
Unit II
Unit III
Unit IV
Unit V
Wangcun
Duibian A
Duibian B
Mo_{EF}
U_{EF}
TOC (%)
P (%)
O2.1
C_{org}/P = 50
C_{org}/P = 2
$[O_2]_{aq}$ (umol^{-1})
$[H_2S]_{aq}$ (umol^{-1})
C_{org} / P

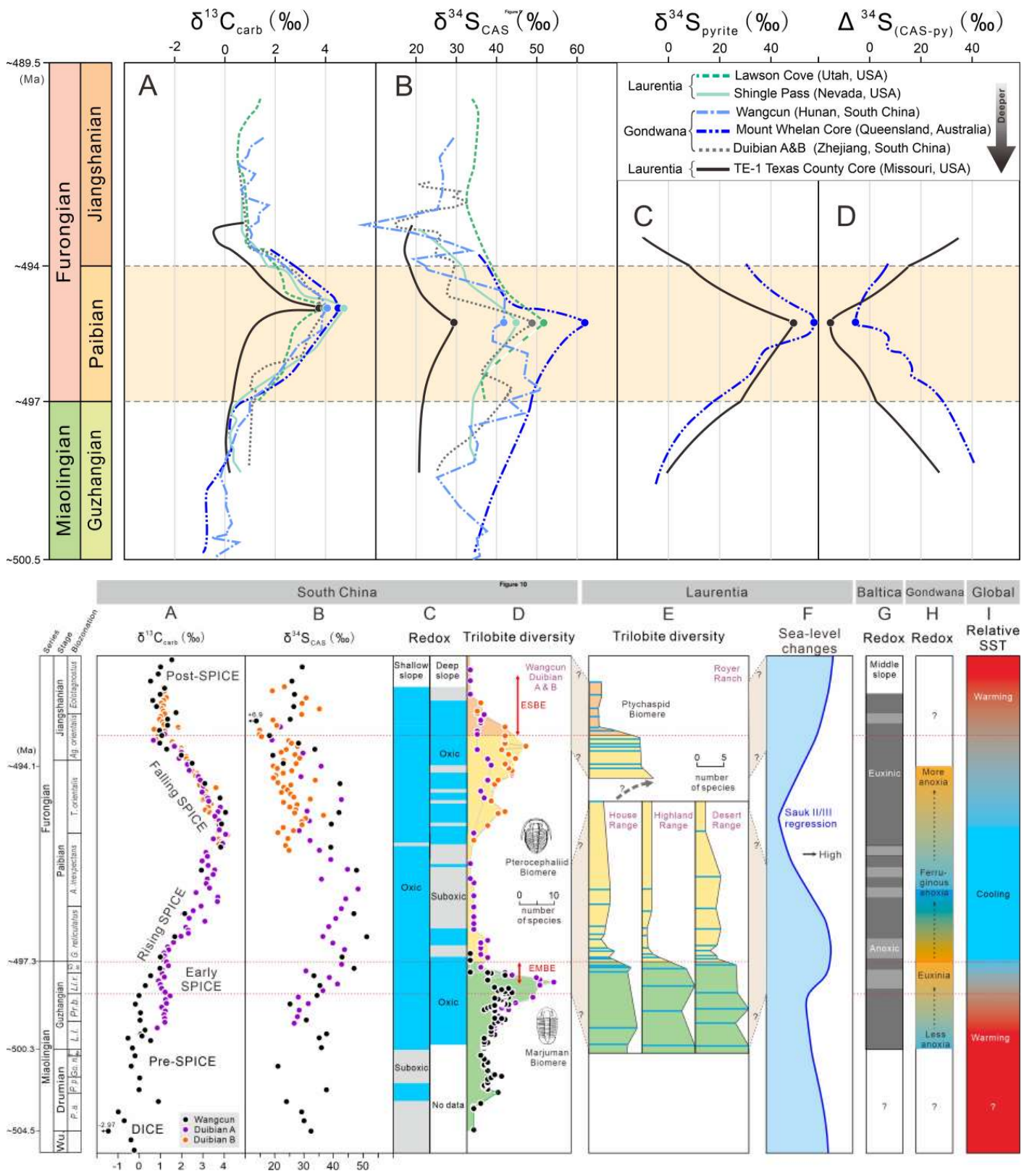
δ13Ccarb (‰)
δ34SCAS (‰)
δ34Spyrite (‰)
Δ 34S(CAS-py) (‰)
A
B
C
D
Laurentia
Lawson Cove (Utah, USA)
Shingle Pass (Nevada, USA)
Gondwana
Wangcun (Hunan, South China)
Mount Whelan Core (Queensland, Australia)
Duibian A&B (Zhejiang, South China)
Laurentia
TE-1 Texas County Core (Missouri, USA)
Deeper
~489.5
(Ma)
~494
~497
~500.5
Furongian
Jiangshanian
Paibian
Miaolingian
Guzhangian
South China
Laurentia
Baltica
Gondwana
Global
Redox
Trilobite diversity
Sea-level changes
Relative SST
Post-SPICE
Falling SPICE
Rising SPICE
Early SPICE
Pre-SPICE
DICE
Wangcun
Duibian A
Duibian B
Shallow slope
Deep slope
Oxic
Suboxic
No data
Wangcun Duibian A & B
ESBE
EMBE
Pterocephaliid Biomere
Marjuman Biomere
Ptychaspid Biomere
Royer Ranch
House Range
Highland Range
Desert Range
number of species
Sauk II/III regression
High
Middle slope
Euxinic
Anoxic
More anoxia
Ferruginous anoxia
Euxinia
Less anoxia
Warming
Cooling
Warming